A DFT based study of the gold-water interface

by

Tshegofatso Titus Masike

A dissertation submitted to the University of the Witwatersrand for the degree of:

Master of Science in Physics

Supervised by

Prof. Gotthard Seifert

and

Prof. Alexander Quandt

2018

Declaration

I, Tshegofatso Titus Masike, hereby declare that the work comprised in this dissertation is my original work, and that any work done by others or by myself previously has been acknowledged and referenced according to the requirements of the Faculty of Science of the University of the Witwatersrand.

Tshegofatso Titus Masike

October, 2019

Abstract

A gold/water interface has been investigated with the DFT-based self-consistent-charge density-functional tight-binding (SCC-DFTB) method using a full cell model with periodic boundary conditions. Born-Oppenheimer molecular-dynamics simulations for water on the surfaces of two Au_{60} electrode slabs were computed. We have demonstrated the applicability of this method to study the structural and dynamical properties of the gold/water interface in a system with periodic-boundary conditions. The results of the simulation clearly show a dependency on the charged electrodes by means of the orientation of the water molecules and the ensuing polarisation of the cell. However, it was also shown that this polarisating effect is confined almost exclusively to first few angstroms away from the electrode . This is indicative of the rather short-range screening behaviour of water. The present study is a feasibility study of models with periodic-boundary conditions and beckons further analysis of metal/electrolyte interfaces on a dependable atomic scale, using periodic boundary conditions.

Acknowledgements

I would like to express my deep gratitude to my co-supervisor, Prof. Alexander Quandt, for introducing me to Solid State Physics and its application to renewable energy systems, and granting me an opportunity to explore these ideas in Germany at Technische Universität Dresden. Thank you for seldom intervening, and allowing me the freedom to explore my own ideas and learn in my own way. I'd also like to express a deeper gratitude to my co-supervisor, Prof. Gotthard Seifert, for recieving me in Dresden, hosting me, and for personally rearing me in the ways of Physical Chemistry. I'll forever be indebted to you for your seemingly never ending patience, even in instances where I did not deserve it.

I'd also like to thank Dr. Robert Warmbier for always bridging the gap of what was expected of me by my supervisors to my understanding and capabilities. Our weekly personal lunch meetings, which I imposed on you, much to the annoyance of you (and your wallet), helped shape my understanding of Theoretical Computational Physics and this dissertation would not have come to fruition, had it not been for you always having high expectations of me. You'd always deny being my supervisor, however, you were my mentor.

Furthermore, I would like to express thanks to the following people:

- Dr. Shinji Hirano for always being willing to explain complex concepts to me when my supervisors were not around.
- The Solid State Physics group at Wits, et al., in particular: Itumeleng Mokgosi and Sandile Kumalo
- The Theoretical Chemistry Group at Technische Universität Dresden.
- The office of P241, et al., in particular: Aymen, Tanita, Ashlynn, Ahmed.

- I'd like to thank and congratulate, recently graduated, Dr. Kai Trepte, for sharing his office space with me in Dresden and teaching me the technical aspects of Computational Physics.

- My friends. Skhathisomusa Dumani Mthembu, Mothusi Sengwatse, Ayanda Bam, Dennis Zheng, Bienvenu Ndagano and Nomaswazi Mthombeni.

- My parents, Mosamo Masike and Dr. Magome Masike, for their never ending support and always allowing me to pursue whatever I wished.

- My siblings, Keitumetse Masike and Tebogo Masike.

I would like to express my gratitude to the Centre of Excellence (CoE) and Materials for Energy Research Group (MERG) for financial support.

We are the scientists, trying to make sense of the stars inside of us.

Christopher Poindexter

Contents

Chapter 1

Introduction

In the context of today's energy production climate, generaton of energy by means of using fossil fuel is currently the most dominant form of energy creation. However, due to the current and projected future energy consumption, and also taking into account an exacerbating environmental problem, there is an urgent need to study and understand the structures of electrochemical interfaces at the atomic level in order to develop clean, efficient electrochemical cells for energy storage and conversion.

Renewable energy creation methods are at a stage, currently, where they are becoming increasingly more efficient at converting natural processes (such as solar energy for example) into clean and usable energy. It has made such progress that the biggest issue concerning renewable energy is not so much about generating electricity but rather finding a means to store it quickly and efficiently. The conventional method of using batteries to store energy has proved to be too slow and inefficient at storing energy from renewable energy systems and has subsequently become the bottleneck process of optimising the renewable energy systems. Batteries are prevalent in electronic devices as they have high energy densities but they discharge energy slowly. Lithium-ion batteries are currently, arguably, the best type of batteries you can get and it is evident as they are becoming increasingly popular and are being used in mobile devices such as phones, tablets and laptops etc. What makes them stand out from other batteries is that they have a higher energy density, they can hold their charge much better, have significantly reduced memory effects, which means that you don't have to completely discharge them before recharging, and a higher amount of discharge/charge cycles as you have to do with other battery

chemistries [1].

Lithium-ion batteries are not without their limitations. Completely discharging a Lithium-ion battery ruins it, they start deteriorating as soon as they leave the factory and they are very sensitive to temperature changes. They require maintenance from time to time and there is a slight chance of spontaneous combustion. All the issues are not specific to Lithium-ion batteries but are issues that plague batteries as a whole [2].

Because batteries generate electricity by converting chemical potential energy to electrical energy. Most batteries have three basic components. Two electrodes (anode and cathode), and an electrolyte. The two electrodes, of two different materials, are immersed into a chemical electrolytic solution, causing chemical reactions to occur at both electrodes. The electrodes react with the electrolyte where charges (ions) gather at the anode (negative electrode) and the charges are pulled away from the cathode (positive electrode) creating a potential difference between the electrodes and thus producing a voltage. The electrodes can be connected to external terminals to supply a current. The pulling of ions through the electrolyte is a corrosive process which creates a different chemical composition in the electrolyte. As it generates power, the chemical composition of the electrolyte alters and as a result the battery's voltage drops slowly and runs flat. In summary, batteries have high energy densities but generally have low power densities, and the materials inside corrode continuously.

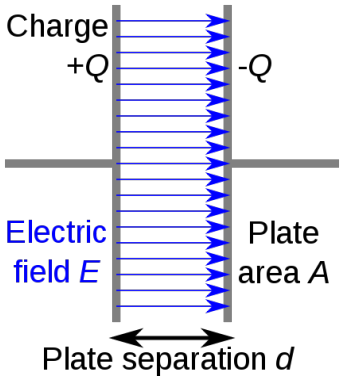

Figure 1.1: Schematic of a capacitor. [3]

Supercapacitors, or capacitors in generally, on the other hand use a completely different process to store energy. Where a battery stores energy chemically, a capac-

itor stores energy electrostatically by applying a potential difference between two metallic plates with a dielectric placed between them, creating an electric field.

A typical supercapacitor differs from a normal capacitor in two aspects. The plates of a supercapacitor have a substantially greater surface area than that of a normal capacitor because the metal plates are coated with a porous substance such as a powdery, activated charcoal for example. Therefore a capacitor can store more charge [4].

In a supercapacitor the dielectric is not the same as it is for a normal capacitor. Instead of having a relatively thick medium made from a kind of ceramic or thin plastic film, both plates of a supercapacitor are soaked in an electrolyte, which is rich in ions, and separated by a very thin insulator membrane. When the plates are charged, oppositely charged ions are attracted to the surfaces, which create an electric double layer whose thickness is approximately in the range of angstroms $\left(1\mathring{A} = 1 \times 10^{-10}\text{metre}\right)$.

$$C = \epsilon_0 \epsilon_r \frac{A}{d} \tag{1.1}$$

Where,

C = Capacitance

A = Area of the two plates

d = Distance between the plates

ϵ_0 = Vacuum permittivity

ϵ_r = The relative static permittivity, of the material between the plates

As one can see from equation

Supercapacitors are classified according to their energy storing mechanisms. The process described above was energy storage mechanism based on electric double layer capacitance (EDLC). However, there exists two more types of supercapacitors. Namely being pseudocapacitors and hybrid capacitors. Pseudocapacitors, unlike EDLCs, have a chemical reaction at the electrode which leads to an electron charge transfer between the electrode and the electrolyte. Hybrid capacitors combine the intercalation process of a lithium-ion battery anode with the double-layer mechanism of the cathode of an EDLC. An example of a hybrid capacitor is the Lithium-ion

capacitor [5].

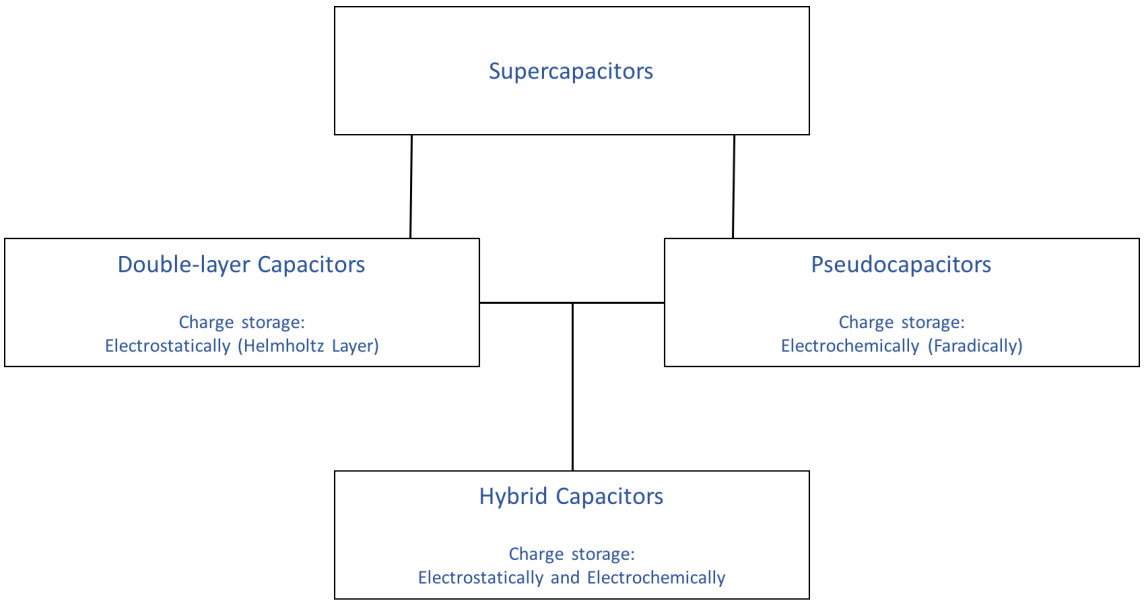

Figure 1.2: Classification of supercapacitors.

By studying metal/electrolyte interfaces on a microscopic but reliable level, we can attain a better understanding of the relationship between the physics that occur at the interface and the ensuing electrostatic potential energy which can be used to calculate the capacitance of the system. Knowledge acquired from this can be used to create better energy storage and be part of a renewable energy system with efficient energy storage [6].

1.1 Capacitor Principles

A capacitor is a great example of how the simplest of technologies, in this case the technologies are an insulator sandwiched in between two conductors, can become an ever increasingly complex technology centuries later. In October of 1745 the Leyden jar was invented by German physicist Ewald Georg von Kleist. However, independently, Pieter van Musschenbroek, a Dutch physicist working at the University of Leyden, discovered the jar a year later in 1746. In the original construction of the Leyden jar, von Kleist used a narrow-neck jar which was partially filled with water and was closed with a cork that had an electrical lead through it which was touching the water at the bottom. Interestingly enough, von Kleist's hands that were holding the jar formed the outer electrode. Once the jar was charged using an electrostatic generator connected to the water, von Kleist gave himself a painful shock by touching the lead to the water whilst still holding the jar. It is reported

that he only did this once. van Musschenbroek's version of the Leyden jar used foil to cover the outside surface of the jar, instead of his hands, to form a less painful, true capacitor. American Benjamin Franklin improved the design by demonstrating that water wasn't essential in making a capacitor and made capacitors which consisted of a sheet of glass between foil electrodes [7]. In the 19^{th} century Michael Faraday was the first to pioneer a practical application of a capacitor whilst he was attempting to store the residual, unused electrons from his experiments and made major contributions to technologies pertaining to capacitors. The biggest of his contributions to capacitor technology is probably introducing the concept of dielectric constant and the invention of the first practical fixed and variable capacitors.

A capacitor is an electrical component that stores energy electrostatically in an electric field. When a charged capacitor is connected to a circuit it may act as a source of voltage for a small amount of time. We find that:

$$C = \frac{Q}{V} \tag{1.2}$$

Where,

C = Capacitance

Q = Charge in the double layer

V = Applied voltage

The capacitance of a capacitor, C, is measured in farads (F). Which is the ratio of the electric charge on each electrode Q to the potential difference V between them. There are two important aspects of a capacitor. Its energy and its power density, which are usually expressed as either a capacitance per unit weight or per unit volume. The energy, E (J), that is stored on a capacitor is correlated to the charge, Q (C), at each electrode and the potential difference, V (V), and thus it is directly proportional to its capacitance [8]:

$$E = \frac{1}{2}CV^2 \tag{1.3}$$

Where,

E = Energy stored in a capacitor

C = Capacitance

V = Potential difference

The energy E increases when V increases. But this trend is usually restricted by a disintegration of the strength of the dielectric.

Another important aspect of a capacitor is its power, (P), which is the rate of energy delivery. In order to determine this we need to take into account the resistance of the internal components of the capacitor (for example the current collectors, electrode materials, dielectric, electrolyte etc.). The resistance of said components are typically measured in aggregate and collectively referred to as the equivalent series resistance (ESR), which is measured in ohms, (Ω). By introducing a voltage drop between the electrodrodes, the ESR dictates what the maximum voltage of the capacitor will be during discharge, which limits the maximum energy and power of a capacitor. The measurement of power for capacitors is measured at a matched impedance (we assume that the resistance of the load is the same as the capacitor ESR) and that is consistent with the maximum power P_{max}, given by:

$$P_{max} = \frac{V^2}{ESR} \tag{1.4}$$

Even though the resistance of a good capacitor is typically much lower than that of the connected load, the actual delivered peak power of the capacitor, which might very well still be high, is usually lower than P_{max}.

1.2 Electrochemical Capacitors

Electrochemical capacitors (ECs) are a unique kind of capacitor based on the charging and discharging rates at the electrode-electrolyte surfaces of high surface area materials. They are ruled by the same principles as normal capacitors, however, they utilise electrodes that have a much higher surface area and the formation of an electrostatic double layer. Such a thin double layer increases both the energy and the capacitance by a factor of almost 10,000 compared to conventional capacitors. Similarly to conventional capacitors, they store electric charge in a highly reversible way and, by maintaining a low ESR, they can be operated at high specific power compared most batteries.

Even though ECs tend to be seen as an alternative to rechargeable batteries in storing/providing electric charge, they use a completely different mechanism of storing charge (i.e. non-faradic or electrostatic, such as in capacitors, vs faradic or chemical, such as in batteries). They can, however, provide rather quick charge and discharge rates relative to batteries (mainly due to the fact that there is no steady chemical processes or phase changes) of a comparable volume size, but their specific energy is less than that of batteries. Thus ECs do have a much higher power density than that of batteries. In combination with very short charge times, longer cycle life, long shelf life, high efficiency (in terms of charge in/charge out). They can be fully charged and discharged without affecting performance or lifetime.

Another important difference between a capacitor and a battery is that there is always an intrinsic increase in voltage on charge and, conversely, an intrinsic decrease on discharge for a capacitor due to the increase or decrease of the charge stored on the electrodes of the capacitor. Batteries have an approximately constant voltage during charge or discharge. The only exception of this is when a battery's state of charge approaches 100%, called top of charge or TOC, or when its close to 0%, called end of charge or EOD. Therefore capacitors will be in need of a DC-DC converter to regulate and stabilise their output. However both batteries and ECs will require an inverter if an alternating current is required.

ECs can be divided into three different kinds of capacitors, based on how they were constructed and how they store energy:

1. The electric double-layer capacitor (EDLC)
2. The pseudocapacitor, also known as the redox EC
3. Hybrid systems incorporating a combination of EDLC and pseudocapacitance

Even though there are several kinds of capacitors which can be constructed out of a myriad of candidate materials and device architectures, the EDLC is the most developed form of EC and this project will be investigating this kind of capacitor.

1.2.1 Electric Double-Layer Capacitors

The concept of the double layer has been around since the nineteenth century. First introduced by von Helmholtz in the nineteenth century when he discovered that charged electrodes immersed in an electrolytic solution attracted oppositely charged ions to their surfaces. Thus two layers of oppositely charged ions form at the interface between the electrode and the electrolyte.

It was not until 1952 that the double layer capacitor was put into practical use in the form of the storage of electrical energy which was demonstrated by H.I. Becker who was working under General Electric. He utilised porous carbon electrodes in an aqueous electrolyte, creating a device that stored charge in the double layer (non-faradically) at the interface between the electrode and the electrolyte solution. In 1966 in a patent by R.A. Rightmire from the Standard Oil Company of Ohio and a follow up patent from the same company by coworker D.L. Boos described a system where energy was stored non-faradically [7]. Nowadays we have quite a number of high performance EDLC devices that are based on porous carbons which are also commercially available from a range of manufacturers for an ever expanding range of applications.

Chapter 2

Theory

2.1 Double Layer Theory

The Double Layer model was created so that one could visualise the ionic movement that occurs in the proximity of a charged surface.

First thing that we have to understand is that matter at the frontier of two different phases (in this case a solid-liquid interface) will have fundamentally different properties from either of the aforementioned continuous phases. The double layer refers to a structure that appears on the surface of an object that is exposed to a electrolytic solution that has two parallel layers of charge confined to it

For instance, when we have a charged surface in our system, there must be a balancing counter charge to counteract the charged surface. This counter charge resides in the liquid - r. one counter charge in the liquid, the charges will not be uniformly distributed throughout the liquid phase but will be clustered close to the charged surface. So we have a section of the liquid phase, albeit a small part, that is different from the extended liquid. This concept is a one of the central themes of electrochemistry and the reactions that occur in this interface are pertinent to external observations of electrochemical reactions.

There are a few theoretical methods of simulating the solid-liquid interface, we will go through a few with emphasis on what they can tell us as opposed to how we need to use them.

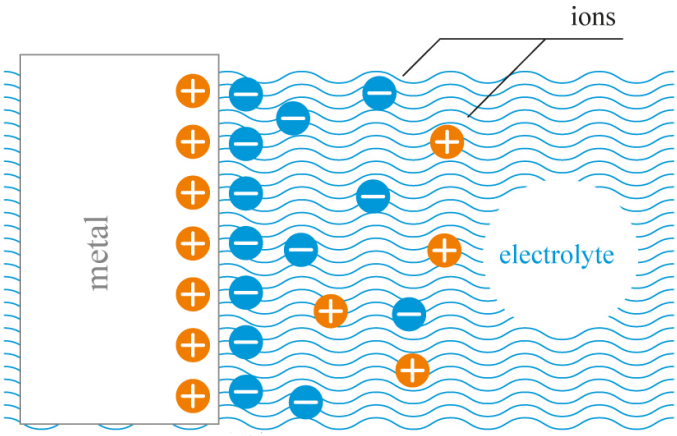

Figure 2.1: Example of a double layer. [9]

2.1.1 Helmholtz Double Layer

Helmholtz was the first to realise that when an electronic conductor is brought into contact with a solid or an electrolyte, a common boundary (interface) between the two phases appears and that two layers of opposite polarity to the conductor form at the boundary of the electrode and electrolyte, essentially being a dielectric on a molecular scale and storing charge electrostatically [10].

This early model is the simplest approximation that the surface charge is neutralised by the oppositely charged ions placed by a small distance away from the surface. The surface charge potential is, in a linear fashion, dissipated from the surface to the oppositely charged ions, satisfying the charge difference.

The Helmholtz theoretical model, although a good basis for the interface, does not adequately describe what occurs in nature as it does not consider instances such as including diffusion/mixing of ions in solution or the account for the possibility of adsorption onto the surface etc. For example it predicts fixed layers of opposite charges, which do not occur in the natural world.

2.1.2 Gouy-Chapman Double Layer

In 1910 Louis Georges Gouy (and in 1913 David Leonard Chapman) observed that the capacitance in the system was not constant but it depended on the applied potential and the ionic concentration [11]. Guoy suggested that the interfacial (boundary)

potential at the charged surface could be ascribed to the presence of a number of the ions of a certain charge attached to its surface and to an equal number of ions of the opposite charge in the solution. Essentially, this means that the oppositely charged ions are not rigidly held, as suggested by the Helmholtz model, but instead tend to diffuse within the liquid phase until they counter the acting potential. The resulting kinetic energy of the oppositely charged ions will, to an extent, affect the thickness of the ensuing double layer. Interestingly enough Gouy and, independently, Chapman developed a model of this "diffuse double layer" in which the change in the concentration of the counter ions clost to a charged surface follows the Boltzmann distribution:

$$n = n_o e^{\frac{-zeY}{kT}} \tag{2.1}$$

Where,

n_o = bulk concentration

z = charge on the ion

e = charge on a proton

k = Boltzmann constant

T = Temperature

Y = Potential

This still does not describe what may be occurring at the interface. The Boltzmann distribution used in this approach is equivalent to the molar concentration in a bulk solution, but this may not hold true near a charged surface. We have a diffuse double layer and not a rigid one, and a more accurate representation of the coulombic interactions between charges would be to look at the volume charge densities instead of the surface charge density. The volume charge density, ρ, can be expressed as:

$$\rho_i = \sum_i z_i e n_i \tag{2.2}$$

The coulombic interaction between charges can be expressed by the Poisson

equation:

$$\frac{d^2\psi}{dx^2} = -\frac{\rho}{\epsilon_r \epsilon_0} \tag{2.3}$$

Where,

ψ = Electric field

ϵ_r = Relative permittivity of the electrolyte solution

ϵ_0 = Permittivity of a vacuum

Where ψ, the electric field, varies from $\psi_{\mathbf{o}}$ at the surface to 0 in the bulk solution. Combining the Boltzmann distribution with the Poisson equation and integrating under the appropriate limits gives the electric potential as a function of distance from the surface. The thickness of the diffuse double layer is given by:

$$L_{double} = \left[\frac{\epsilon_0 \epsilon_r kT}{2n_o e^2 v^2}\right]^{\frac{1}{2}} \tag{2.4}$$

Where,

$v^2 = \sum_i n_{io} z_i^2$ (Cation valency)

From the equation above, one can see that the double layer thickness decreases as the valency and/or the concentration increases and the double layer increases as the relative permittivity of the electrolyte solution (dielectric constant) increases.

In a nutshell, the Gouy-Chapman theory describes a rigid charged surface with a cloud of oppositely charged ions in the solution and the concentration of the oppositely charged ions decreasing with the distance from the surface, which is the diffuse double layer. This theory is better than the Helmholtz Double Layer theory, however, it still has its limitations and doesn't adequately describe reality. Experimentally the thickness of the double layer is found to be greater than the expected thickness, which stems from the use of an equilibrium Boltzmann distribution. It also speaks towards the fact that both anions and cations exist in the solution, and the further away you move from the surface, the more that ions with the same charge as the electrode surface will be found within the double layer as well.

2.1.3 Stern Modification of the Diffuse Double Layer

As discussed above, the Gouy-Chapman theory gives a better description of reality than the Helmholtz theory but it does have its own limitations. The greatest limitation is the assumption that ions behave as point charges, when in reality there are no physical limits for the ions in their approach to the surface. In 1924 Otto Stern realised this and modified the Gouy-Chapman diffuse double layer [12]. In his theory he stated that ions have a finite size and so they cannot approach the surface closer than a few nanometers. Thus the first ions of the Gouy-Chapman Diffuse Double Layer are not at the surface, but at some distance away from the surface.

Stern did assume that some of the ions are specifically adsorbed by the surface in the plane **d**, and this surface becomes what is known now as the Stern Layer. Therefore, the potential will drop by $\mathbf{A_o} - \mathbf{A_d}$ over a molecular capacitor, also known as the Helmholtz Plane and by the Stern Layer, $\mathbf{Y_d}$, over the diffuse layer.

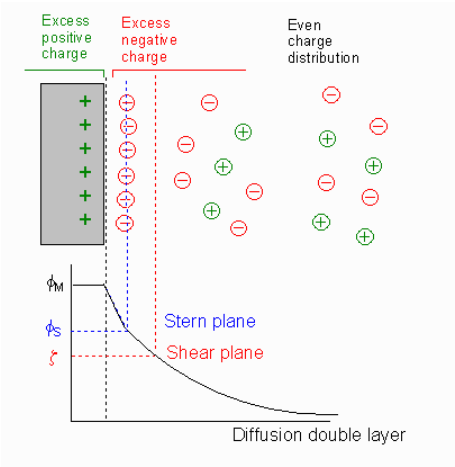

Figure 2.2: In this diagram we are comparing the amount of counterions in both the Stern Layer and the Diffuse Layer. [13]

The double layer is formed to neutralise the charged surface which causes an electrokinetic potential between the surface and any point in the mass of the suspending liquid, this voltage difference is often referred to as the surface potential. As we move away from the surface, the potential drops off almost linearly in the Stern layer and then it drops off exponentially through the diffuse layer, tending to zero at the imaginary boundary of the double layer. This potential is quite useful as it indicates the strength of the electrical force between the particles and the distance at which this force influences the double layer.

A charged particle will move with a fixed velocity in a voltage field, this phenomenon is called electrophoresis. The mobility of the charged particle is related to the dielectric constant and viscosity of the suspending liquid and, on the electric potential at the boundary between the moving particle and liquid. This boundary is called the *slip plane* and is defined as the point where the diffuse layer and the Stern layer meet. Figure 2.2 above shows the change in charge density through the diffuse layer.

2.2 Approximate Density Functional Theory and Density Functional Tight Binding Theory

Density-functional tight binding (DFTB) theory is an approximate density functional method [14], based on density functional theory (DFT) as formulated by Hohenberg and Kohn [15]. It is an extremely powerful method for the calculation of the physical and chemical properties of molecules, clusters and condensed matter systems in their ground state. DFT is a theory where a many-body wave function is replaced with an electron density $n(\vec{r})$, as a basic entity. Using an electron density, in many cases, is much easier than wave function methods due to the fact that it reduces the many-body problem of N electrons with $3N$ spatial coordinates to only three spatial variables by the use of functionals. Using an electron density, which only has 3 spatial variables, and thus is far less computationally expensive than using wave function methods. Therefore DFT and DFTB can be applied to much larger systems with far more atoms.

Currently we have efficient DFT-(Kohn-Sahm, KS) computer codes and access to computer clusters which allows for the studying of systems with increasing size and complexity. However, the size of time and length scales, which is demanded in simulations nowadays, is growing faster than the acceleration of DFT computer codes or the increasing hardware technologies can compensate for. As a result of this, there will be the need of even faster and approximate methods which permit studying large systems with small computational effort or short simulation times. Until recently, classical force fields methods (molecular mechanics, MM), were applied for this purpose, because they are many orders of magnitude faster than DFT (Hartree-Fock,

HF). Although the disadvantages of using classical force field methods are their exceptionally limited transferability from one system to another, unavailability of accurate force field parameters and their incapacity to consider quantum effects.

Semi-empirical quantum chemical methods are faster than DFT(Hartree-Fock), but slower than molecular mechanics. Semi-empirical quantum chemical methods contain a number of element specific parameters, where as in DFT there are no adjustable parameters whatsoever as it is an ab initio method. The rule of thumb is that the more adjustible parameters you have in a method the less physical or accurate it becomes the upside, however, is speed. Even though these parameters require a reasonable effort in their determination to ensure their transferability, SE methods can describe nearly all quantum effects attainable by DFT (with few exceptions) [16].

Empirical tight-binding methods are the corresponding counterparts of the SE quantum-chemical methods in the condensed phase. In the 1980s, it was shown that a 'TB' scheme, which is the application of an atom-specific basis-set representation, can be used as the basis for a more meticulous treatment within the essense of DFT-KS.

These early ideas have been further developed during the past 20 years and lead to the development of density-functional tight-binding (DFTB) methods. The DFTB method is as computationally efficient as empirical tight-binding methods but it is more closely related to DFT. The DFTB method has already been applied to study large biomolecules, clusters, nanostructures and condensed-matter systems with a broad range of elements. Below we will briefly revisit the important technical aspects of *Density Functional Theory* and *Density Functional Tight Binding Theory.*

2.2.1 Approximate Density Functional Theory

The total energy within Density Functional Theory can be written as:

$$E_{tot}\left[n\left(\vec{r}\right)\right] = T\left[n\left(\vec{r}\right)\right] + E_{ext} + E_H + E_{nn} + E_{xc}\left[n\left(\vec{r}\right)\right] \tag{2.5}$$

Where,

T = Kinetic energy of the electrons

E_{ext} = Electron-nuclei interaction energy

E_H = Hartree interaction energy

E_{nn} = Nuclear interaction energy

E_{xc} = Functional of the xc (exchange correlation) energy

The electron density, $n(\vec{r}) = \sum_i \psi_i^*(\vec{r})\,\psi_i(\vec{r})$, or for the sake of simplicity can be refered to as n, is obtained by using the solutions of the Kohn-Sahm equations:

$$\left[-\frac{1}{2}\nabla^2 + V_{eff}(\vec{r})\right]\psi_i(\vec{r}) = \epsilon_i\psi_i(\vec{r}), \qquad V_{eff} = V_{ext} + V_H + V_{xc} \tag{2.6}$$

Where,

$$V_{ext} = -\sum_j \frac{Z_j}{r_j}\vec{r}, \qquad V_H = \int \frac{n(\vec{r}')}{|\vec{r} - \vec{r}'|}d\vec{r}, \qquad V_{xc} = \frac{\delta E}{\delta n} \tag{2.7}$$

V_{eff} = Effective potential of the electrons

V_{ext} = Electron-nuclei interaction potential

V_H = Hartree interaction potential

V_{xc} = Exchange correlation potential

By using the Kohn-Sahm equations, Eq. (2.6), we can express the total energy as:

$$E_{tot} = \sum_i \langle\psi_i|-\frac{1}{2}\nabla^2 + V_{eff}|\psi_i\rangle - \frac{1}{2}\left[\int V_{eff} n d\vec{r} - \int V_{ext} n d\vec{r}\right] + E_{xc}[n] - \frac{1}{2}\int V_{sc} n d\vec{r} + E_{nn} \tag{2.8}$$

We can take $\hat{h}^0 = -\frac{1}{2}\nabla^2 + V_{eff}$.

The total energy, E_{tot}, is variational with respect to the density variations in the system and because of this, the total energy can be calculated from an approximate electronic charge density. The approximate density can be found if one knows the approximate density distribution in the system. In this text we will refer to this reference density as n_0, which should be as close as possible to the exact density, and we will refer to as $\tilde{n}$, but can be further refined. To implement this we equate

the exact density to the sum of the reference density and a density fluctuation: $\tilde{n} = n_0 + \delta n$. Now we are going to expand the energy at the reference density, so $n = n_0$, up until the second order in the density fluctuations of δn. The total energy may now be written as:

$$\begin{aligned} E_{tot} = &\sum_i \langle\psi_i|\hat{h}^0|\psi_i\rangle + \int\int \left(\frac{1}{|\vec{r} - \vec{r}'|} + \left.\frac{\delta^2 E_{xc}}{\delta n \delta n'}\right|_{n=n_0} \right) \delta n \delta n' d\vec{r} d\vec{r}' \\ &- \frac{1}{2}\left[\int V_{eff} n_0 - \int V_{ext} n_0\right] + E_{xc}[n_0] - \frac{1}{2}\int V_{xc} n_0 + E_{nn} \end{aligned} \tag{2.9}$$

A well educated guess for the reference density could be that it is a superposition of the atomic densities in the system. If we take this "guess" seriously $n_0(\vec{r}) = \sum_j n_j^0(\vec{r})$. Correspondingly, the effective potential can be written as a superposition of atomic contributions: $V(\vec{r}) = \sum_j V_j(\vec{r})$, as well as the exchange-correlation (xc) term:

$$E_{xc} - \frac{1}{2}\int V_{xc} n = \frac{1}{2}\int V_{xc} n - \int n^2 \frac{\delta \varepsilon_{xc}}{\delta n} = \frac{1}{2}\sum_j \sum_k \left[\int V_{xc,j}^0 n_k^0 - 2\int n_j^0 n_k^0 \frac{\delta \varepsilon_{xc}}{\delta n^0}\right] \tag{2.10}$$

So by plugging in Eq. (2.10) into the total energy:

$$\begin{aligned} E_{tot}(\tilde{n}) \approx &\sum_i \langle\psi_i| -\frac{1}{2}\nabla^2 + \sum_j V_{eff,j} |\psi_i\rangle + \frac{1}{2}\int\int \left(\frac{1}{|\vec{r} - \vec{r}'|} + \left.\frac{\delta^2 E_{xc}}{\delta n \delta n'}\right|_{n_0} \right) \delta n \delta n' \\ &- \frac{1}{2}\sum_j \sum_k \int V_{eff,j}^0 n_k^0 + \frac{1}{2}\sum_j \sum_k \left[\int V_{xc,j}^0 n_k^0 - 2\int n_j^0 n_k^0 \frac{\delta \varepsilon_{xc}}{\delta n^0}\right] \\ &- \frac{1}{2}\sum_j \sum_k \int \frac{Z_j}{r_j} n_k^0 + \frac{1}{2}\sum_j \sum_{k \neq j} \frac{Z_j Z_k}{R_{kj}} \end{aligned} \tag{2.11}$$

The electron-nuclei interaction integral can be simplified by a point-charge approximation for large interatomic distances:

$$\frac{Z_j}{r_j} n_k^0 \approx \frac{Z_j Q_k}{R_{kj}} \qquad \text{where} \quad j \neq k \qquad \text{and} \qquad Q_k^0 = \int n_k^0 \tag{2.12}$$

For large distances, the atomic population converges to the nuclear charge: $Q_k \to Z_k$. This holds true for uniform nuclear systems and non-uniform nuclear systems. As a result of this, for large distances it is realised that the nuclear-nuclear

repulsion energy term and the electron-nuclear attraction energy term in Eq. (2.11) complement each other. Another consequence of being in the large distance range is that the two-center terms, which contain the potential, disappear. This occurs because the reference density and the neutral atomic potential (i.e. the superposition of the neutral atomic potential contributions) w_j^0 decay at an exponential rate as we go further away from the nuclei. At distances $\overrightarrow{R_l}$ and $\overrightarrow{R_j}$:

$$\sum_j \sum_k \int w_j^0 n_k^0 = 0 \qquad where \quad l \neq j \tag{2.13}$$

Furthermore, by using the same line of reasoning, we can assume that:

$$\int V_{xc,j}^0 n_k^0 = 0 \qquad \text{and} \qquad \int n_j^0 n_k^0 \frac{\delta \varepsilon_{xc}}{\delta n^0} = 0 \qquad where \quad l \neq j \tag{2.14}$$

All the many-center terms (where $l \neq j$) in the second line of Eq. (2.11) disappear at large interatomic distances.

Now, if we assume - as we have done before - that the density is described by a superposition of atomic densities ($\delta n \to 0$), then the total energy is simply the sum of the Kohn Sahm single particle energies with the addition of the one-center terms (where $l = j$) from Eq. (2.11). Taking all these expressions into consideration, we have:

$$\begin{aligned} E_j(n_j^0) = &\sum_i^{N_j} \langle \psi_i^j | -\frac{1}{2}\nabla^2 + \sum_j V_{eff,j}^0 | \psi_i^j \rangle - \frac{1}{2} \int V_{eff,j}^0 n_j^0 \\ &+ \frac{1}{2} \left[\int V_{xc,j}^0 n_j^0 - 2 \int n_j^0 n_j^0 \frac{\delta \varepsilon_{xc}}{\delta n^0} \right] - \frac{1}{2} \int \frac{Z_j}{r_j} n_j^0 \end{aligned} \tag{2.15}$$

Where N_j is the number of electrons and ψ_i^j are the atomic orbitals of the jth atom in the system.The binding energy is approximately given by the simple relation:

$$E_B = E_{tot} - \sum_j E_j \approx \sum_i \tilde{\varepsilon}_i - \sum_j \sum_{l \in j} \varepsilon_l^j \tag{2.16}$$

$$\text{Where,} \quad \sum_i \tilde{\epsilon}_i = \sum_i \langle \psi_i | \hat{h}^0 | \psi_i \rangle \qquad \text{and} \qquad \varepsilon_l^j = \langle \psi_l^j | -\frac{1}{2}\nabla^2 + \sum_j V_{eff,j}^0 | \psi_l^j \rangle \tag{2.17}$$

As the interatomic distances decreases, the assumption where we assumed large atomic distances doesn't hold anymore, and as a result of this the compensating terms in Eq. (2.11) are calculated by using the atomic densities and potentials and are then reconciled with the nuclear repulsion energy terms into a sum of pairwise repulsive energy terms:

$$
\begin{aligned}
&-\frac{1}{2}\sum_{j}\sum_{k\neq j}\int V^{0}_{eff,j}n^{0}_{j}+\frac{1}{2}\sum_{j}\sum_{k\neq j}\left[\int V^{0}_{xc,j}n^{0}_{k}-2\int n^{0}_{j}n^{0}_{k}\frac{\delta\varepsilon_{xc}}{\delta n^{0}}\right]\\
&-\frac{1}{2}\sum_{j}\sum_{k\neq j}\int \frac{Z_j}{r_j}n^{0}_{k}+\frac{1}{2}\sum_{j}\sum_{k\neq j}\frac{Z_jZ_k}{R_{kj}}\\
&\Rightarrow \sum_{j}\sum_{k\neq j}V_{rep,kj}\left(R_{kj}\right)
\end{aligned}
\tag{2.18}
$$

In short interatomic distances, the nuclear repulsion overshadows the other contributions in the system so the pairwise energy terms of Eq. (2.18) are all repulsive in this limit.

The two-center coulomb contribution to the term in $\delta n\delta^{'}$ in Eq. (2.11):

$$
\int\int\left(\frac{1}{|\vec{r}-\vec{r}^{\,\prime}|}\right)\delta n_j\delta n^{'}_{k}\quad\text{with}\quad k\neq j \tag{2.19}
$$

This will now be represented as the second order term in E_{second} which can be accounted for in a multipole expansion where one only considers the monopolar terms in Δq_j. If we relate the second order energy term of an atom to the change of the state of charge of the atom, we can make the following approximation:

$$
E_{second}\approx\frac{1}{2}\sum_{jk}\chi_{kj}\left(\left|\vec{R}_k-\vec{R}_j\right|\right)\Delta q_j\Delta q_k \tag{2.20}
$$

Where the atomic charges $\Delta q_k=Q_k-Q^0_k$ and χ_{kj} are shorthands for the second derivative of the Hartree Fock and xc contributions.

Taking all approximations into consideration, we ultimately find that the total energy now becomes:

$$
E_{tot}\approx\sum_{i}\varepsilon_i+\frac{1}{2}\sum_{k}\sum_{j}\chi_{kj}\left(\left|\vec{R}_k-\vec{R}_j\right|\right)\Delta q_j\Delta q_k+\sum_{j}\sum_{k\neq j}V_{rep,kj}\left(R_{kj}\right)+\sum_{j}E_j-\sum_{j}\sum_{l\in j}\varepsilon^{j}_{l} \tag{2.21}
$$

2.2.2 Approximate Kohn-Sahm Equations

$$\left(-\frac{1}{2}\nabla^2 + \sum_j V^0_{eff,j} + V_{second}\right)\psi_i = \tilde{\varepsilon}_i\psi_i \tag{2.22}$$

Where $\hat{h^0} = -\frac{1}{2}\nabla^2 + \sum_j V^0_{eff,j}$ and $\hat{h^1} = V_{second}$

Eq. (2.22) relates the approximate density $\tilde{n}$ and the expression for the total energy Eq. (2.21) with the Kohn-Sahm like equation. The ensuing effective potential, V_{eff}, is composed of the sum of the atomic potentials $V^0_{eff,j}$ (refer to Eq. (2.11)) and the corresponding contributions which are related to E_{second}. The explicit expressions for the aforementioned contributions will be given in the next section within a representation of linear combinations of atomic orbitals (LCAO) for the Kohn-Sahm orbitals.

2.2.3 The LCAO approach: 'Tight Binding'

In the LCAO perspective, the Kohn-Sahm oribitals can be written as:

$$\psi_i(\vec{r}) = \sum_\nu^N C_{i\nu}\phi_\nu \tag{2.23}$$

This equation is related to the corresponding secular equations:

$$\sum_\nu^N C_{i\nu}\left(H_{\mu\nu} - \varepsilon_i S_{\mu\nu}\right) = 0 \tag{2.24}$$

The matrix elements are given by:

$$\begin{aligned} H_{\mu\nu} &\equiv \langle\phi_\mu|\hat{h}^0 + \hat{h}^1|\phi_\nu\rangle \\ &= \langle\phi_\mu|\hat{h}^0|\phi_\nu\rangle + \frac{1}{2}S_{\mu\nu}\sum_k^N\left(\chi_{jk} + \chi_{kl}\right)\Delta q_k \\ &= H^0_{\mu\nu} + H^1_{\mu\nu} \quad \forall\ \mu\ \in\ l,\ \nu\ \in\ j \quad \text{with} \quad S_{\mu\nu} = \langle\phi_\mu|\phi_\nu\rangle \end{aligned} \tag{2.25}$$

As you can see, the matrix elements $H^0_{\mu\nu}$ are determined by $\hat{h}^0$ from Eq. (2.22). The orbitals in Eq. (2.22) are portrayed in a minimal basis of optimised atomic orbitals, represented by the pseudoatomic basis functions, φ_μ, which are acquired by solving the Kohn-Sahm equations for a spherically symmetric, spin-unpolarized

neutral atom self-consistently.

$$\left[-\frac{1}{2}\nabla^2 + V^0_{eff,j} + \left(\frac{r_j}{r_0}\right)^{n_0}\right]\varphi_\mu = \varepsilon_\mu \varphi_\mu \tag{2.26}$$

A contraction potential has been introduced to Eq. (2.22), in the form of $\frac{r_j}{r_0}^{n_0}$ where $n_0 = 2$, in order to formulate a more efficient basis set for molecular and solid state systems. Initially introduced by Eschrig and others. [17], [18]

In order to restrict the basis to solely valence orbitals, it is essential to ensure orthogonality of the basis functions with respect to the core basis functions of the system. The valence orbitals, as they are solutions to Eq. (2.2.3), are orthogonal to the core orbitals of the same atom, however, this doesn't apply to all other atoms. Orthogonality to the core orbitals of all of the other atoms in the system can be achieved by:

$$|\phi_\mu\rangle = |\phi_\mu) - \sum_{k\neq j}\sum_a |\phi^k_a)(\phi^k_a|\phi_\mu), \quad \mu \in j. \tag{2.27}$$

In Eq. (2.27), $|\phi_\mu)$ is the atomic orbital μ at atom j, $|\phi^k_a)$ are solutions of Eq. (2.2.3) and are the corresponding core orbitals at atom k. If we initiate the orthogonalisation procedure to calculate the matrix elements $H^0_{\mu\nu}$, we will get:

$$H^0_{\mu\nu} = (\varphi_\mu| - \frac{1}{2}\nabla^2 + \sum_j V^0_{eff,j}|\varphi_\nu) - \sum_l\sum_{cl}(\varphi_\nu|\varphi_{cl})\varepsilon_{cl}(\varphi_{cl}|\varphi_\mu), \qquad \mu,\nu \not\in l. \tag{2.28}$$

Where ε_{Cl} is the energy of the core state at center l. This potential $V^0_{eff,j}$, together with its core state correction in Eq. (2.28), can be seen as a pseudopotential but only for atoms, on which the basis functions φ_μ and $varphi_\nu$ are not centered. Therefore the pseudopotential is only seen in the three center terms. So for φ_μ at j and φ_ν at k, where $j \neq k \neq l$ and in the supposedly crystal-field-like terms, which occur at both φ_μ and φ_ν at $j, j \neq l$, of the matrix elements $H^0_{\mu\nu}$. Whereas the 'true' potential $V^0_{eff,j}$ is present in the rest of the other terms. Now, if we assume a 'weak' pseudopotential, this leads us to a two centerapproximation for the Hamilton matrix elements:

$$H^0_{\mu\nu} = (\varphi_\mu| - \frac{1}{2}\nabla^2 + V_l + (1-\delta_{lj})V_j|\varphi_\nu), \qquad \mu \in j, \quad \nu \in l. \tag{2.29}$$

After the two center approximation, Eq. (2.29), which now contains two center terms solely, has the same structure of the secular equations in Tight Binding schemes or the extended Hückel method, however, this is advantageous because all matrix elements are calculated within DFT. Introduced [19] and then further discussed [14] by Gotthard Seifert.

$H^1_{\mu\nu}$ in Eq. (2.25) are the second order contributions to $H_{\mu\nu}$ and only consist of two center terms. Due to this the entire Hamilton and overlap matrices contain one and two center contributions only. Consequently, they can be calculated and tabulated prior to any simulation as functions of the distance between atomic pairs. Thereby circumventing any need to recalculate any integral during an actual calculation. The pairwise tabulated integrals only now have to be transformed to the specific coordinate system of the basic functions which are the atomic orbitals. [20]

For the charge density, $n(\vec{r}) = \sum_i \psi_i^*(\vec{r})\,\psi_i(\vec{r})$, the atomic charges ($\Delta q_j$) in matrix elements $H^1_{\mu\nu}$ are dependent on orbitals φ_i via the KS ansatz. Because of this dependency, the eigenvalue problem in Eq. (2.24) has to be solved self-consistently. This self-consistency requirement has to be achieved for the charges (Δq_j) of the atoms in the system, this restricted self-consistency is called a self-consistent charge (SCC) treatment. This self-consistency requirement also occurs in a 'full' DFT calculation, however, contrary to the LCAO tight binding approach, the self-consistency has to be achieved for the entire charge density and not just for the charges of the atoms in the system solely.

Obtaining the charge of an atom in a molecule or solid is not trivial as it is not uniquely defined. Consistent with the minimal valence basis ansatz for the Kohn-Sahm orbitals, the simplest approach is to define the charges by way of projecting the atomic orbitals to each atom. The parting of the overlapping contributions can easily be done with the Mulliken approach and the ensuing charges correspond to the Mulliken Charges.

After solving the approximate Kohn-Sahm equations, the binding energy can be calculated by using Eq. (2.21) and the repulsive energy contributions can be calculated by using Eq. (2.18). However, in practice, the pairwise contributions are

fitted to full Density Functional Theory calculations, in essence, any high sufficiently complex calculation could be used. The pairwise repulsive energy contributions, for example, can be fitted to the following type of polynomials. [21]

$$V_{rep}(R) = \begin{cases} \sum\limits_{n=2} d_n \left(R_c - R\right)^n, & \text{for} \quad R < R_c, \\ 0, & \text{otherwise.} \end{cases} \tag{2.30}$$

Thus the repulsive potential contributions must be fitted to each pair of elements and not for each pair of atoms. Once calculated, it can be tabulated as the Hamilton and the overlap matrix elements. The value V_{rep}, is known to be quite well transferable between different systems. This is due to the repulsive terms being characteristicly short range, for example, the term R_c is of the order of approximately 1.5 times of the usual interatomic bonding distance.

Forces acting on the atoms in the system can also be analytically expressed:

$$\vec{F_j} = -\frac{\partial E}{\partial \vec{R_j}} = -\sum_i^M \sum_{\mu\nu}^N C_{i\mu} C_{i\nu} \times \left[\frac{\partial H^0_{\mu\nu}}{\partial \vec{R_j}} - \left(\epsilon_i - \frac{H^1_{\mu\nu}}{S_{\mu\nu}} \right) \frac{\partial S_{\mu\nu}}{\partial \vec{R_j}} \right] - \Delta q_j \sum_l^N \frac{\partial \gamma_{jk}}{\partial \vec{R_j}} \Delta q_l - \frac{\partial V_{rep}}{\partial \vec{R_j}} \tag{2.31}$$

One should take note that the calculation of the derivatives of the Hamilton and the overlap matrices can be performed quickly and efficiently, due to the integrals being stored in tables. This is essential for the actualisation of molecular-dynamics (MD) simulations with the DFTB approach. This numerical differentiation has proven to be pragmatic and approximate.

Chapter 3

Computational Details

In this work, all SCC-DFTB calculations were executed by using the DFTB+ code [22]. The *auorg-1-1* [23] parameter set was used, which are essentially an extension of the *mio-1-1* Slater-Koster files with an inclusion of gold atoms. The Born-Oppenheimer DFTB molecular dynamics simulations were implemented within a canonical framework. Newtons equations of motion were calculated and integrated by using the *Velocity Verlet* algorithm, and a time step of *0.3 fs* was used to ensure reversibility. To avoid the desorption, as discussed in Xiaohang Lin's paper [24], of superficial water, as we want to maintain the neutral structure of the water molecules (and desorption of water is unphysical in this case), a *Nosé -Hoover thermostat* was implemented at a constant low temperature of *180 K*. The system evolved for 5.0 ps. Snapshots of the system were taken after every *30 fs*, giving us a total of 55 snapshots of the system.

The set-up used to study the gold/electrolyte interface is under periodic boundary conditions. Explicitly charging the system with DFTB+ causes the total energy of the system to diverge. To avoid this, two ions of opposite charge are included in the system and due to the presence of the two ions, there is an electron transfer between the ion and the surface of the electrode. Doing this causes the system to be charged implicitly and enables us to study the interfacial region between the electrode and electrolyte, thereby alleviating the need of charging it explicitly in the first place. In order to charge this system, we implanted one H_3O^+ molecule, close to the left-hand side electrode, and one OH^-, close to the right-hand side electrode, to induce an electron transfer and create a potential difference between the two elec-

trodes thus charging the system whilst ensuring that the total energy of the system does not diverge.

The surface of the two electrodes are that of a bulk face-centered cubic (111) surface of Au_{60} which sandwiches bulk water - with a chosen density of $1g.ml^{-1}$ - that is randomly distributed and orientated, as described above. The minimum distance between the electrode and a water molecule is $2,72$Å which is the sum of the Van Der Waals radii' of $O_{rw} = 1.52$Å and $H_{rw} = 1.2$Å. After optimisation of the geometry using SCC-DFTB+ algorithm *Conjugate Gradient*, a molecular dynamics simulation was performed, as described above as well.

3.1 Geometry

To create the geometry of the gold/water interface cell, the ASE program (Atomic Simulation Environment) [25] was used to define the in-plane basis vectors and cell repetitions for the gold electrode. The model system used is a slab that comprises a full cell capacitor system with gold as the material chosen for the electrodes and water as the electrolyte, that is periodic in the x, y and z directions with approximately 10 Å vacuum on either side between the electrode and the border of the cell - a diagram will follow later in this chapter. The slab consists of two electrodes - each electrode is 9,462 Å thick, has five layers of Au(111) in the z-direction and each layer has 12 gold atoms - on either side of the system and the electrolyte, which is randomly but equally distributed water molecules, in between the two electrodes.

x	y	z
0	0	0
8,651	0	0
0	9,999	0
0	0	106,875

Table 3.1: Cell parameters of the system.

The cell parameters, i.e. the dimensions of the system, Systems that have a metal/water interface are known for being notoriously difficult to simulate with periodic boundary conditions, this is because it is easy for such systems to become unstable from, perhaps, an unbalanced charge in the system which can cause a dipole moment to occur. This dipole moment, now an artefact in each iteration,

continues to grow and, due to having to account for periodic boundary conditions, causes the total energy of the system to diverge. Even a small dipole moment in a system with periodic boundary conditions, can, likely, cause the system to implode as the cumulative residual charge increases as the system repeats itself. Taking this problem into account, a full cell capacitor system was chosen that was "symmetric" and well distributed so that no spurious charge imbalance could implode the system during the molecular dynamics simulations. Idealy, periodicity would have only been accounted for in the directions of the x- and y-axis and not for the z-axis, however this is not possible, not only for the DFTB+ code, but in almost all available DFTB based programs, this is more of a conceptual problem when making DFTB based codes and not a technical shortfall. It could possibly be "solved" with Green's function techniques. But as this is not the case for the DFTB+ code, it was accounted for by inputting some vacuum space between the cell parameter walls and the gold electrode along the z-axis.

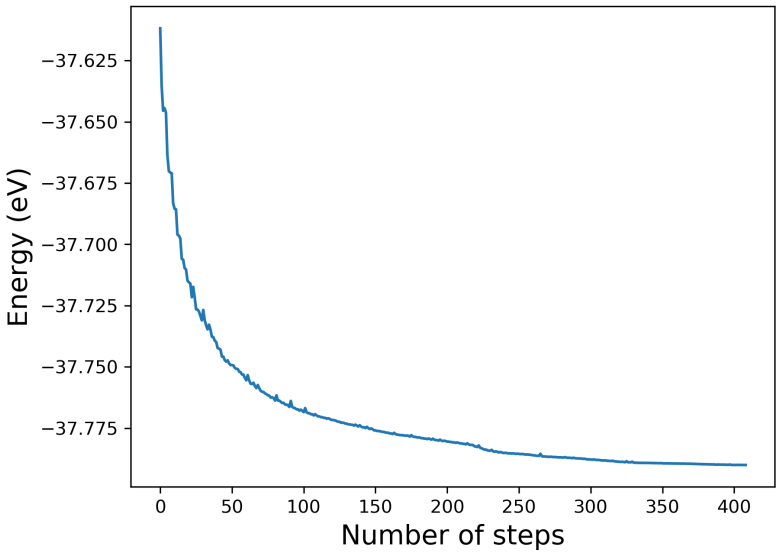

Figure 3.1: Graph of energy per atom after geometry optimisation.

To optimise the geometry, the *Conjugate Gradient* algorithm was implemented until the total energy per atom in the system converges. As you can see from **??**, after a few hundred iterations the total energy per atom converges to a single value, which in this case is -37.80 eV. The negative value for the energy means that the system is in a bound state. Using this method gives us an approximate but effective way of judging how well defined the dimensions of the geometry of the system are, in spite of many approximations being present. Generally, a geometry is optimised until it reaches a minimum energy threshold, this was not the case here. In our

case, a geometry was optimised to the point where the total energy per atom is clearly converging to a single value. The computational cost of running a longer optimisation to get a more "accurate" position of the atoms in the system is too high considering how negligible the change in the total energy per atom will be.

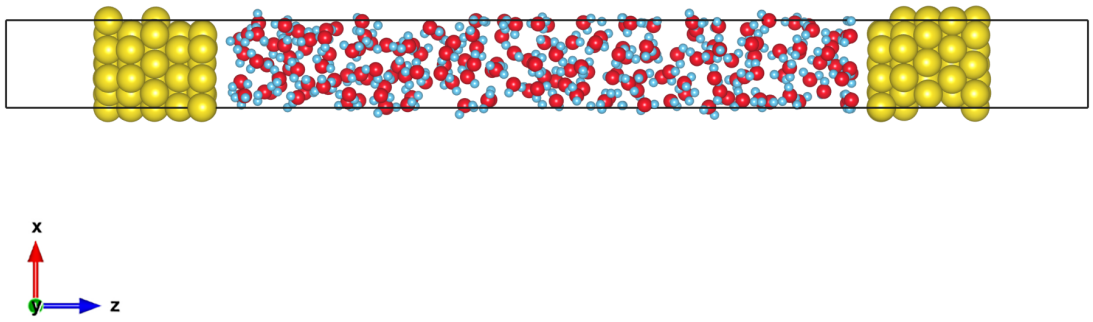

Figure 3.2: Snapshot of the $2Au_{60}$ + $183H_2O$ + H_3O^+ + OH^- system on the XZ-plane.

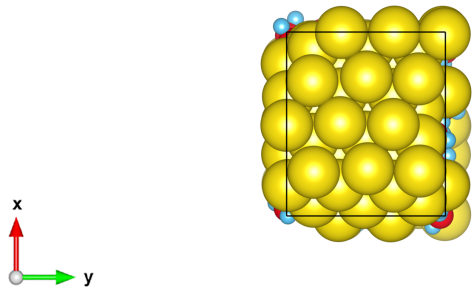

Figure 3.3: Snapshot of the $2Au_{60}$ + $183H_2O$ + H_3O^+ + OH^- system on the XY-plane.

The black outline in the above figures are to illustrate the boundaries of the cell. To account for not being able to charge the system explicitly, as this would further induce a dipole moment, two oppositely charged ions, hydronium (H_3O^+) and hydroxide (OH^-), are placed in the AuH_2OH_3OOH system. The hydronium is placed 37,298 Å away from the origin on the z-axis and the hydroxide is placed 70,370 angstrom, the ions are strategically placed to be the same distance away from the center of the system. This is done to ensure that the ions are equidistant from each other with respect to the z-direction and that it still holds when the periodic

boundary conditions are taken into account so that there is "symmetry" - at least prior to the electron transfer - in the cell and will help to negate the presence of spurious dipole moments which could cause the total energy of the system to diverge.

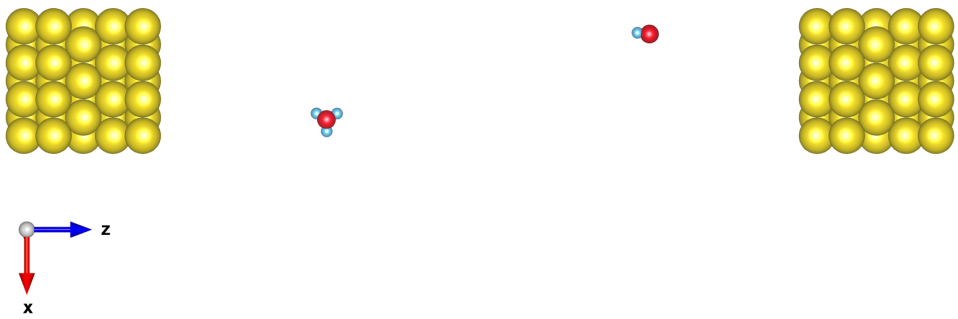

Figure 3.4: Snapshot of the $2Au_{60}$ + H_3O^+ + OH^- system, which is our model system without water and only the ions to showcase the position of the ions in the system.

3.2 Molecular Dynamics Scheme

Analytical solutions denote exact solutions to problems. However, more often than not, an analytical solution only exist for very few practical systems in the universe. That is why we use the numerical approach to approximate a practical result. One example of such a case is Molecular Dynamics Simulations [26] (MD), where we integrate the classical equations of motion to generate the trajectories of a system with N particles in time. The N particles are denoted by $3N$ coordinates, which are the position and momenta in a three dimensional volume space. If we let particle i be subjected to a force $\vec{f}_i$ at a time t. MD simulations solve Newton's equations of motion:

$$\frac{d^2\vec{r}_i}{dt^2} = \frac{\vec{f}_i(\vec{r}_1, \vec{r}_2, \vec{r}_3)}{m_i} \tag{3.1}$$

Where force $\vec{f}_i$ is dependent on the particle's positions and, consequently, velocities. The forces are based from the Tight-Binding Density Functional Theory [27]

A MD simulation generally follows this algorithm:

1. At time $t = 0$ the system is initialised by choosing positions and velocities of the particle. A value is also chosen for Δt, which is the time step that is used in the numerical integration of Newton's equations of motion.

2. Calculate the forces of all the particles in the system.

3. Newton's equations of motion are integrated using a suitable integration scheme. Once this is done, the positions and the velocities of particles at $t + \Delta t$.

4. Return to step 2.

MD is a deterministic method by nature, which is known as cause-and-effect, in contrast to Monte Carlo [28] simulations which are stochastic and thus random. Given an initial condition a MD simulation will always reach the same trajectory in phase space. In MD simulations physical properties are calculated from time averages along certain trajectories. Take $X\left(\vec{r}_N(t), \vec{v}_N(t)\right)$, its average value can be found by:

$$\langle X \rangle = \frac{1}{N} \sum_{n=0}^{N-1} X\left(t_0 + n\Delta t\right) \tag{3.2}$$

Where,

t_0 = Initial time of the system. X = A physical quantity dependent on position and velocity

Generally a physcial quantity is charaterised by some relaxation time, sometimes denoted by τ, which is the time one has to wait until system X reaches an average equilibrium value.

3.2.1 Velocity Verlet

One of the most widely used integration schemes is the *Velocity Verlet* [29] algorithm- along with its precursor the *Verlet* algorithm- where the positions and velocities are updated concurrently:

$$\vec{r}_i\left(t + \Delta t\right) = \vec{r}_i(t) + \vec{v}_i \Delta t + \frac{\vec{a}_i(t)}{2} \Delta t^2 + O(\Delta t^4) \tag{3.3}$$

$$\vec{v}_i\left(t + \Delta t\right) = \vec{v}_i(t) + \frac{\vec{a}_i(t + \Delta t) + \vec{a}_i(t)}{2} \Delta t \tag{3.4}$$

One advantage of the Velocity Verlet algorithm is that it is a fully time reversible scheme. A reversion invariant scheme is helpful because you can integrate forward first and then integrate backwards with the same method and constant time-step length, you will pass through the same points of the numerical trajectory in the reverse order, making it an even function [30]. Another advantage of using the Velocity Verlet algorithm is that it is a *sympletic integrator* [31]. Symplectic integrator algorithms have the characteristic where their trajectories conserve a quantity called a "pseudo energy" which represents the true energy but differs by only a small amount, which vanishes as $\Delta t \to 0$. How this helps within the frame of molecular dynamics is that there won't be long time deviations of the trajectories from the real trajectories, which can happen due to the accumulation of numerical errors during the time evolution of the simulation. [32]

A reasonable time step is required for a physically feasible MD simulation, such that the simulation is long enough to be relevant to the time scales of a natural process being studied but also small enough to avoid discretization errors. To avoid such errors, one must always ensure that the time step (Δt) is smaller than the fastest vibrational frequency/phenomenon.

Chapter 4

Results and Discussion

To get insight on the gold/electrolyte interface, we studied the distribution functions $g(r)$, the orientations of the OH bonds, the charge distribution and the electrostatic potential of the system, which will also be discussed in detail further on. To analyse the data adequately, we took snapshots of the system as it evolved throughout the Molecular Dynamics simulation (MD), averaged the statistics of each snapshot by superimposing them over one another and analysing that entire system. The ergodic hypothesis [33] was used to better our dataset by equating the space average to time average. It is a common feature in the repertoire amongst computational physicists.

4.1 Charge Distribution

The charge distribution of a system is very important because it tells us under what conditions the system is in and from that we can get an intial idea on how the system will act, or react, after being disrupted.

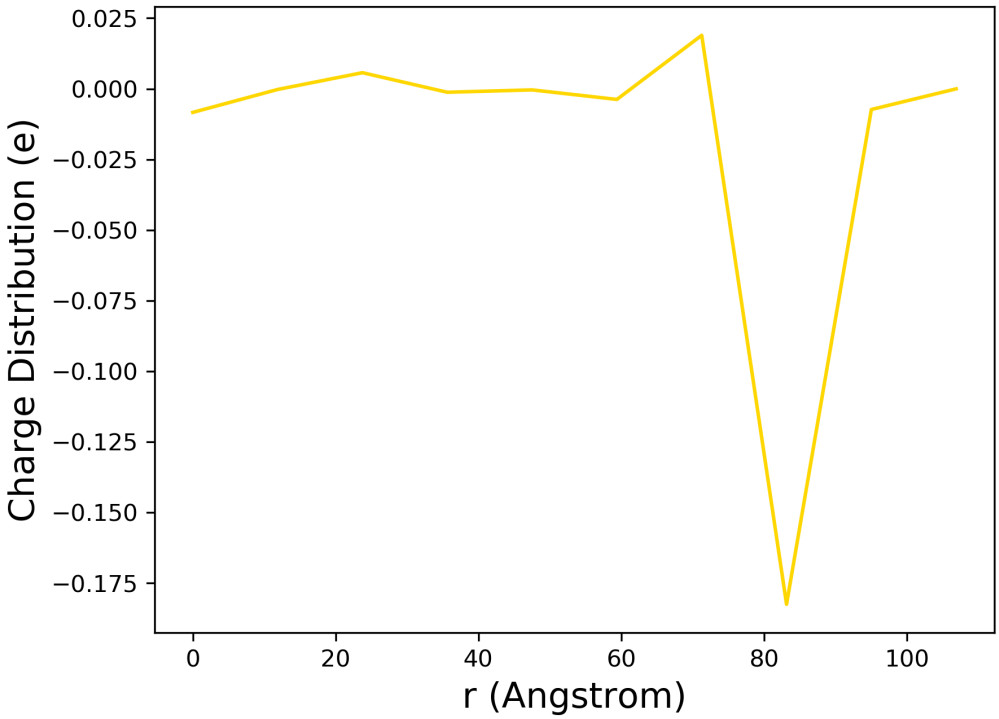

Figure 4.1: Charge distribution of the system.

The charge distribution graph, Figure 4.1, was calculated by averaging the charges along the x- and y- direction, and map them onto the z- direction using the final snapshot of the MD simulation. The gold electrodes are each approximately 10 Å thick and are found in regions 9,975 Å $<$ z $<$ 19,437 Å and 86,533 Å $<$ z $<$ 95,780 Å.

There are two events that we should pay special attention to in Figure 4.1 - one at 23,76 Å and the other at 70,37 Å. These points in the graph indicate changes in the charge distribution in the system, the first peak is approximately where the first Au electrode-water interface is. The increase and drop in charge indicates that there is a very slight potentional across the interface and that slight drop continues until we come across the H_3O^+ ion which was placed at approximately 37,298 Å. This region however has remained neutral for the most part until we start approaching 60 Å where the charge distribution becomes more positively charged until approximately

70,37 Å - where the OH^- was placed - from there until approximately 83,87 Å there is a drastic potential drop. The increase and decrease in the charge distribution in this region is indicative of an electron transfer that occurred between the right Au electrode interface and the anion. The charge transfer achieves the desired effect and the system - or at least the right electrode - has now become charged and this is evidence of that.

4.2 Electrostatic Potential

The electrostatic potential is necessary to calculate the capacitance of a system. The electrostatic potential is found by calculating the electrostatic potential on a grid, averaging the values for the electrostatic potential along the x- and y- direction and superimposing these values along the z- axis. DFTB+'s newly included electrostatic potential function was very helpful in this regard.

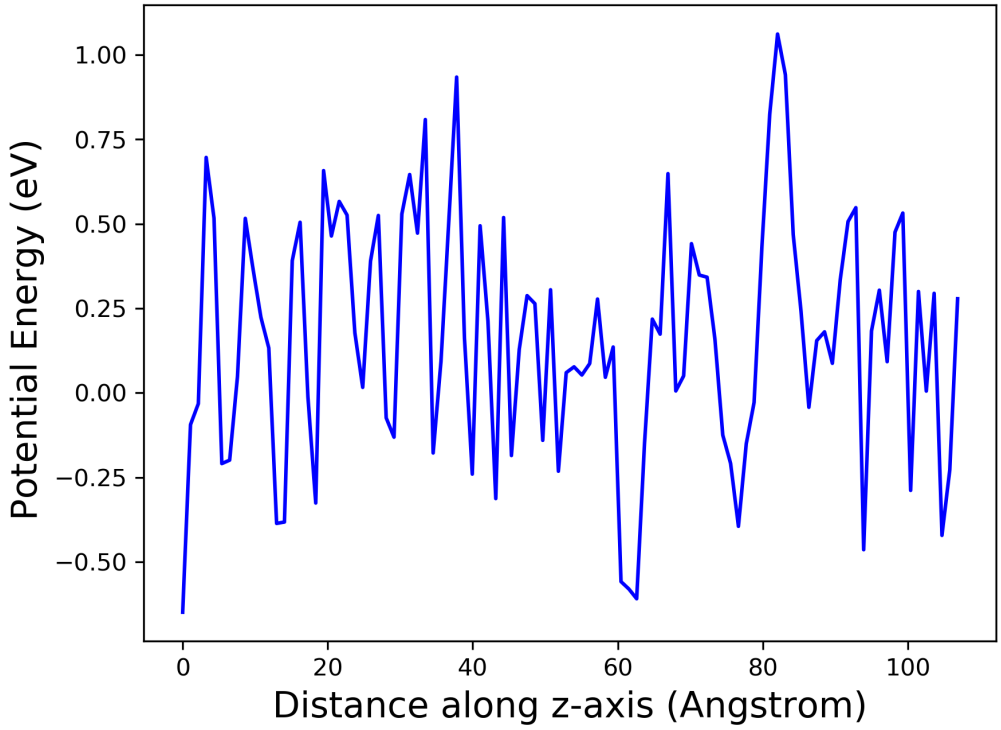

Figure 4.2: Electrostatic potential of the system.

From Figure 4.2, its hard to discern anything meaningful at first glance. This is mainly because the atomic charges Δq_j in $H^1_{\mu\nu}$ depend on the orbitals psi_i by means of the Kohn-Sahm ansatz for the charge density $n(\vec{r})$ and due to this, the eigenvalue problem in Eq. (2.24) must be solved self-consistently. However, the self consistency need not be attained for the charge density, but only for the charges Δq_j

of the atoms in the system. What this does is "localise" the charge, as compared to a "full" self-consistent DFT calculation. This affects the granularity, i.e. the charge distribution represented on a grid and, subsequently, the electrostatic potential. The atomic charges are, effectively, localised in contrast to a fully self-consistent charge density. What this results in is that the atomic charges which are calculated within this formulism have a strong influence on the electrostatic potential. Which then becomes very sensitive to the size of the grid that is used, a procedure that is not always well defined and, to an extent, also non-physical.

This does not mean, however, that one cannot gain any kind of information by exploring the corresponding electrostatic potential.

If you pay special attention to the peak at 82,78 Å, with the highest potential energy, you will see that it is situated very close side electrode was placed. This corresponds to the electrode being charged due to its charge transfer with the OH^- ion in the system. Just before the approximate place where the H_3O^+ (70,37 Å) was placed, we see that the potential energy of the system was relatively stable, which is typical for the electrostatic potential of bulk water. On the far left and far right of the graph - where the Au electrodes are placed - it is admittedly difficult to make out the arrangement of the electrode layers. This is due to the granularity of the algorithm used to calculate the potential in addition to the localisation of charges which was mentioned above. In the region of 9,562 Å $< z <$ 19,87 Å, where the first electrode was approximately placed, there are 3 peaks and 2 troughs. The drops and increases in potential between these peaks are a result of the empty space between each of the gold layers. The same can be said about the Au electrode on the far right of the system in the region of 86,533 Å $< z <$ 95,780 Å. Except for that fact that the Au electrode on this side is more interesting because of the charge transfer - making it negatively charged - and as a result the potential energy distribution is not as "temperate" as the first Au electrode.

4.3 Distribution Function $g(r)$

The distribution function is a histogram where certain distance intervals (measured from in between the surfaces of the electrodes) are treated as bins for the number of atoms that are found within that specific interval. In this body of work, there were 100 bins or intervals with a size of 1.07 Å. This is done so that we can have

a general understanding of where most of the atoms gather during a molecular dynamics simulation and then deduce why they move in that particular way. The gold atoms were not accounted for in the radial distributed function because they are mostly stationary and do not move around as much as the water molecules do. The gold surfaces are located at 19.4Å and at 86.5 Å respectively.

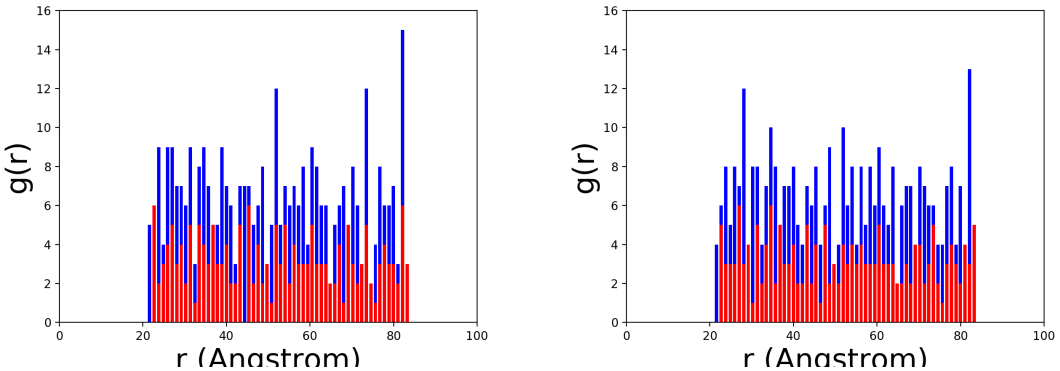

(a) Initial configuration.

(b) Final configuration.

Figure 4.3: The initial vs. final distribution functions for the corresponding configurations of the model system after 16667 steps. The red represents oxygen atoms and the blue represents hydrogren atoms.

Figure 4.3a shows the radial distribution function of the geometry of the system pre-MD simulation and figure 4.3b shows the function post-MD simulation. The most noticeable difference between the two graphs is that figure 4.3b does not have as many peaks as 4.3a where as in Figure 4.3a has two instances of such a configuration. Throughout the MD simulation, due to having a constant temperature thermostat, the water molecules have evened out into the system and are occupying more horizontal orientations than they did in Figure 4.3a. The electron transfer that occurred has also created a new atomic environment such that the orientations of the water molecules correspond to an energetically more favourable configuration.

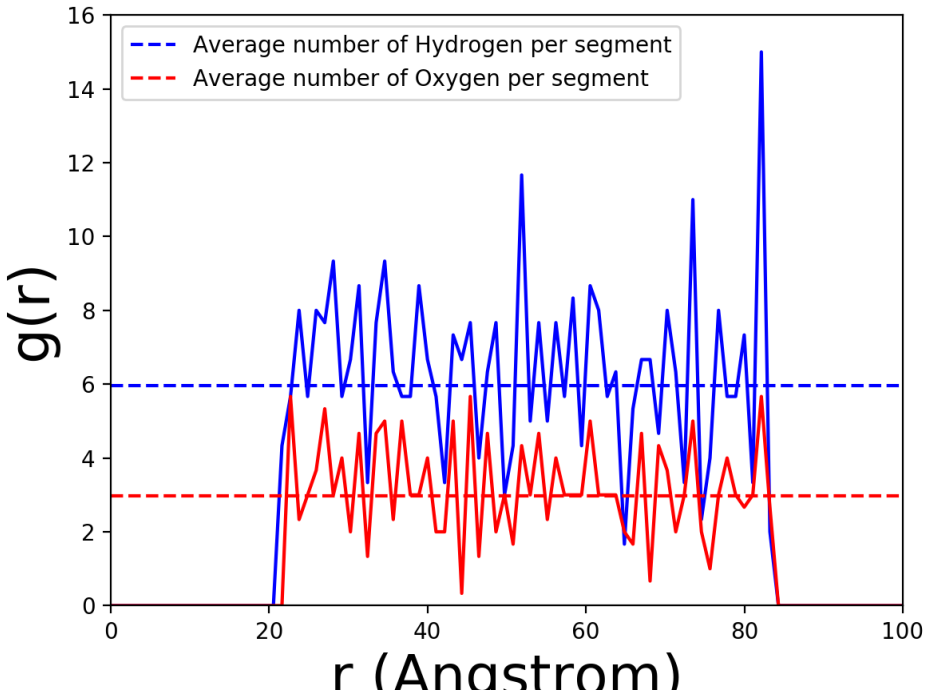

Figure 4.4: Water molecule distribution function of the system averaged over the snapshots of the MD trajectory. All data points are averages from the MD simulation. The red represents the oxygen atoms and the blue represents the hydrogen atoms.

Figure 4.4 shows the average number of oxygen and hydrogen atoms in each interval of the system. The figures document the evolution of the general position of each atom in the system and what one immediately sees is that there is a strong concentration of water molecules adjacent to the right-hand side electrode. The charge distribution in the system, with a neutral charge (or slightly positively charged) on the left-hand side electrode and a negative charge on the right-hand side electrode, is such that it polarises the cell. Once the electric field in the cell is polarised, the water molecules in the system re-orientate themselves according to this field. As a result we have a great number of water molecules migrating to the right-hand side of the cell and virtually no migration to and around the left-hand side of the cell. Note that though water molecules are neutral as a whole, they are polar molecules. Thus the oxygen side of the water molecule is slightly negatively charged and the hydrogen side of the water molecule is slightly positively charged. This is consistent with there being a negatively charged electrode on the right-hand side of the electrode because the positively charged side of a water molecule is the side with the two hydrogen atoms, which both carry a positive partial charge. Owning to the electrostatic force of attraction between the negatively charged electrode and the

positively charged side (hydrogens) of the water molecules, not only do you see a migration of water molecules to the right-hand side electrode, you also observe a lateral spreading of the water molecules so that they are no longer "on top of each other" as they previously were, but they tend to maintain a horizontal state as seen in Figure 4.3. In the next section we'll further investigate the orientation of the water molecules as a result of being present in a charged system.

4.4 Orientation of the OH bonds

To study the orientation of the water molecules with respect to the surface(s) of the gold electrode surfaces similar to previous studies, [34], we determine a probability distribution function $logP(cos\theta)$, where θ is the respective angle between an OH bond and a vector pointing from the oxygen atom to the gold electrode surface. In addition to that, a histogram of the orientations that OH bonds may occupy is extracted from our studies. The value for θ was calculated by using:

$$cos\theta = \frac{\vec{u} \cdot \vec{v}}{||\vec{u}|| \cdot ||\vec{v}||} \tag{4.1}$$

Where $\vec{u}$ is the vector pointing from the electrode surface plane, which it is normal to, to an oxygen atom and $\vec{v}$ is the vector from the oxygen atom to the hydrogen atom. OH bonds which are orientated parallel to the electrode surface, i.e. where the OH bond ($\vec{v}$) is 90° away from the vector ($\vec{u}$), are considered to be type I OH bonds. OH bonds where the value of θ is greater than 90° are bonds where the hydrogen atom is pointing towards the electrode surface (i.e. type II bonds) and OH bonds where the value of θ is smaller than 90° are bonds where the hydrogen atom is pointing away from the electrode surface (i.e. type III bonds). One can see a simple illustration of the three types of bonds in figure 4.5 below.

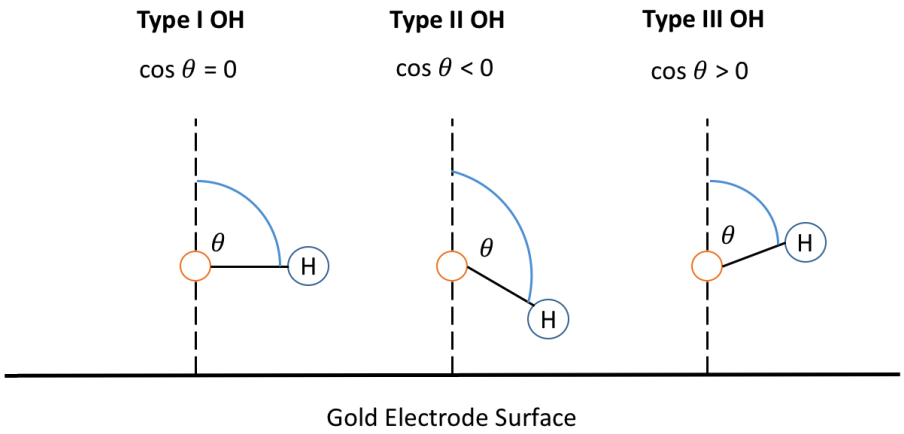

Figure 4.5: OH bond orientation types in a solvation layer of the gold surface. Angle θ is the angle between an OH bond and a vector from the gold surface plane, which it is normal to, to the corresponding oxygen atom.

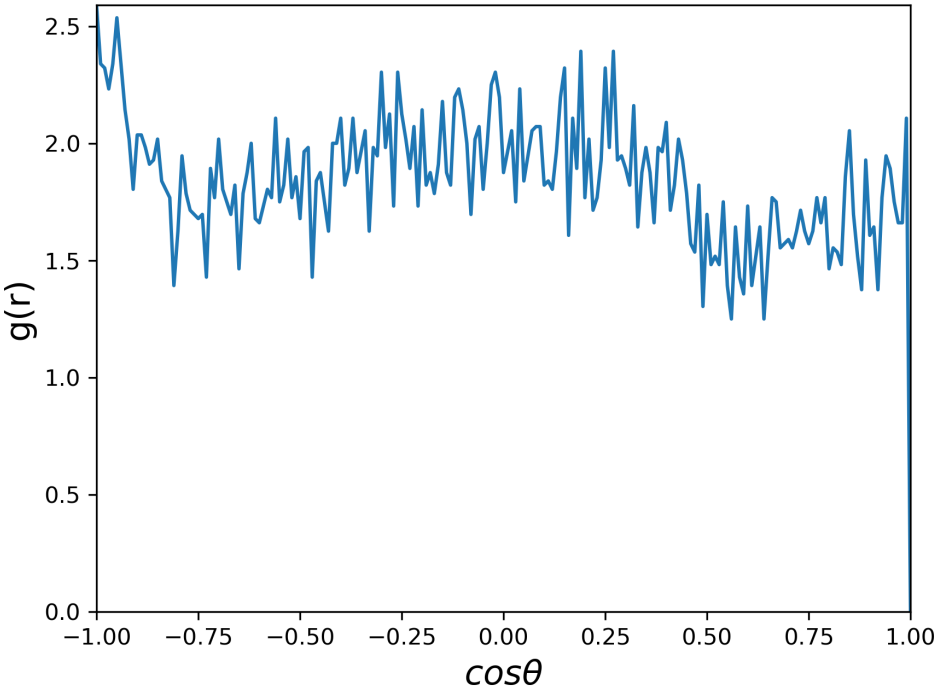

Figure 4.6: Orientation histogram of the system averaged over the snapshots of the MD trajectory.

Figure 4.6 shows us the average number of OH bonds that occupy certain orientations in the system. From what we can observe from Figure 4.6, OH bonds that occupy orientations within the range of approximately $-0.50 < cos\theta < 0.50$ are dominant in the system. However, they represent the bulk water molecules in the system, which are water molecules that are typically not close to either of the electrodes, and are weakly polarised by the system being charged. Orientations that are least represented fall within the range of approximately $0.50 < cos\theta < 1$, these

orientations represent OH bonds where the hydrogen atom is pointing away from the gold electrode surface, which is expected due to the absence of a postively charged electrode.

This type of behaviour is expected within the region closest to the left-hand side electrode because it is furthest away from the negatively charged right-hand side electrode. Water molecules that were within the immediate proximity of the right-hand side experienced the greatest change in OH bond orientation because the electrostatic force of attraction is inversely proportional to the square of the distance. Due to this inverse proportionality, the closer two charges are to each other, the greater the force. And in this case it translates to certain OH bonds orientating with the hydrogen side of the hydrogen bond being closest to the negatively charged electrode. It is noteworthy to mention that in Figure 4.6 there are absolutely no OH bonds that have an orientation of $cos\theta = 1$, where the OH bond is perpendicular to the gold electrode surface with the hydrogen atom pointing away from it. Note that in the very same system we have the most likely OH bond be that of an orientation of $cos\theta = -1$, where the OH bond is perpendicular to the gold electrode surface with the hydrogen atom pointed directly towards it, is again indicative of a system that has been charged and the water molecules are reacting to this environment.

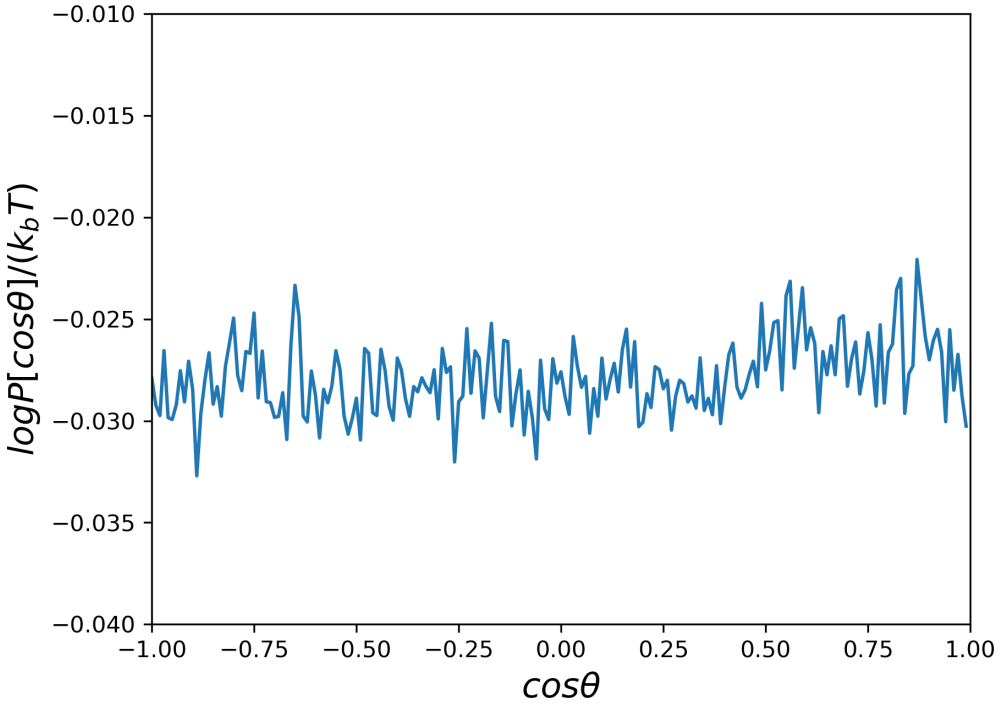

Figure 4.7: Probability distribution $P(cos\theta)$ of the system averaged over the 56 snapshots of the MD trajectory.

The probability distribution of the system can be seen in Figure 4.7. What is peculiar about this distribution is that it looks completely random. There are no significant extrema and so this represents, essentially, bulk water that is randomly distributed and randomly orientated, where all orientation states are equiprobable. This is unprecedented as all our other results indicate, at the very least, that in a charged cell there will be a tendency for certain orientations of OH bonds to occur more than others.

According to past computational studies, [35] [34], we have seen that in the limit T tends to 0 and within full relaxation that the OH bonds close to the metal surface will orientate themselves such that the proton will be pointing towards the negatively charged gold surface. However, in our cell we have a competing artifact, i.e. the counter electrode. The counter electrode has produced frustrating effects across the cell as it is "positively" - albeit not strong but still present - charged whilst its counter part is negatively charged, due to the electron transfer. The frustrations posed are such that polarised water molecules will feel an additional, repulsive electrostatic force. Though weak, the counter electrode can still mitigate many water molecules from being polarised truly by one source. Running the MD will always act as a smoothing force if we keep the temperature the same throughout the MD, which we did. The "smoothing force" in this case, seems to have smoothed the orientation of bulk water molecules in such a way that the observed polarisation effects that occured in the system have been swept away by the MD simulation. Once the electron transfer has occurred during the simulation, the water in the system, collectively, became positively charged as the OH ion surrendered its electron to the gold electrode. This positively charged bulk water created an attenuation of the electrostatic force generated by the negatively charged electrode, thus almost exclusively polarising the water molecules closest to the negatively charged electrode, creating a polarised solvation layer. This further demonstrates the short ranged screening behaviour of bulk water.

For each of the ions in the system, the screening is different because the interaction with the surrounding water is different. The overrall system is neutral, and the internal charges differences will be redistributed during the MD simulation but not in a symmetric fashion. The screening of the electrostatic forces comes from

the hydrospheres surrounding the ions. The hydrospheres of each of the ions in the system have a unique effective dielectric constant (ϵ) caused by the molecular dipoles of the water molecules forming the local hydrospheres.

Please note that:

$$D \equiv \epsilon E + P \tag{4.2}$$

Where,

D = Displacement field

ϵ = Effective dielectric constant

E = Local electric field

P = Polarisation density

From Eq. (4.2) it is evident that the displacement electric fields of the two ions in the system will, in general, be different and because they are different one cannot expect to see a perfectly symmetric screening of oppositely charged ions between the two electrodes. This is typical behaviour of water molecules being polarised within a charged system.

Chapter 5

Conclusion and Future work

Within the scope of this work, we have demonstrated the pertinance of SCC-DFTB in studying the structural and dynamical properties of gold/water interface using a model with periodic boundary conditions which is essentially an extenson of the work done by Gianluca - in his case he looked at the gold/water interface of a cluster model [34]. The studied cell consisted of $2Au_{60}$ + $183H_2O$ + H_3O + OH with vacuum space on either side of the cell to act as a screening medium between each cell (periodic boundary conditions). The two ions were placed in the system to induce an electron transfer and thus charge the system. After a geometry optimisation of the cell, molecular-dynamics simulations were performed (5.0 ps) and the MD trajectories were analysed by means of a charge distribution, radial distributions, probability distributions and molecular orientations.

The results thereof clearly show a charge dependent orientation and, consequently, the polarisation of the layer of water adjacent to the negatively charged gold electrode where the OH bonds were orientated with the hydrogen atoms being closest to the electrode surface and the oxygen atom being furthest away from it. What this work also reveals, however, is the short-ranged screening behaviour of the water molecules. The results from this work are also consistent with a recent experimental study by Tong *et al* [36] where it was found that water molecules tend to be orientated with their OH groups pointing towards ($cos\theta < 0$) the Au metal surface. The present study was a feasibility study of metal/electrolyte interfaces on a reliable atomic level in models with periodic boundary conditions.

For future work, the possibility are almost endless as previously many computational physicists shied away from studying systems with periodic boundary conditions as its very easy for the total energy of the system to diverge. For one, running the same simulation but with a longer simulation time so that the system is allowed to evolve for a longer amount of time, thus creating more snapshots and thus give us more data to analyse to have a more thorough look of the cell. Provided that the Slater-Koster files exist, any material can be used as a potential electrode in virtually any setup.

Bibliography

[1] Steven G Chalk and James F Miller. Key challenges and recent progress in batteries, fuel cells, and hydrogen storage for clean energy systems. *Journal of Power Sources*, 159(1):73–80, 2006.

[2] John B Goodenough and Kyu-Sung Park. The li-ion rechargeable battery: a perspective. *Journal of the American Chemical Society*, 135(4):1167–1176, 2013.

[3] Shamima Nasreen, Gregory M Treich, Matthew L Baczkowski, Arun K Mannodi-Kanakkithodi, Yang Cao, Ramamurthy Ramprasad, and Gregory Sotzing. Polymer dielectrics for capacitor application. *Kirk-Othmer Encyclopedia of Chemical Technology*, pages 1–29, 2000.

[4] B E_ Conway. Transition from "supercapacitor" to "battery" behavior in electrochemical energy storage. *Journal of the Electrochemical Society*, 138(6):1539–1548, 1991.

[5] Marin S Halper and James C Ellenbogen. Supercapacitors: A brief overview. *The MITRE Corporation, McLean, Virginia, USA*, pages 1–34, 2006.

[6] Rizwan Ahmed and Jan Rossmeisl. First principle simulations of electrochemical interfaces-a dft study. 2015.

[7] Janet Ho, T Richard Jow, and Steven Boggs. Historical introduction to capacitor technology. *IEEE Electrical Insulation Magazine*, 26(1), 2010.

[8] Brian E Conway. *Electrochemical supercapacitors: scientific fundamentals and technological applications*. Springer Science & Business Media, 2013.

[9] Alexander Fridman and Lawrence A Kennedy. *Plasma physics and engineering*. CRC press, 2004.

[10] David C Grahame. The electrical double layer and the theory of electrocapillarity. *Chemical reviews*, 41(3):441–501, 1947.

[11] GH Bolt. Analysis of the validity of the gouy-chapman theory of the electric double layer. *Journal of Colloid Science*, 10(2):206–218, 1955.

[12] Keith B Oldham. A gouy–chapman–stern model of the double layer at a (metal)/(ionic liquid) interface. *Journal of Electroanalytical Chemistry*, 613(2):131–138, 2008.

[13] New Mexico State University. Electric double layer, 2017. Online; accessed June 12, 2017.

[14] G Seifert. Tight-binding density functional theory: An approximate kohn- sham dft scheme. *The Journal of Physical Chemistry A*, 111(26):5609–5613, 2007.

[15] Pierre Hohenberg and Walter Kohn. Inhomogeneous electron gas. *Physical review*, 136(3B):B864, 1964.

[16] Gotthard Seifert and Jan-Ole Joswig. Density-functional tight binding—an approximate density-functional theory method. *Wiley Interdisciplinary Reviews: Computational Molecular Science*, 2(3):456–465, 2012.

[17] Helmut Eschrig. Optimized lcao method and the electronic structure of extended systems. *Optimized LCAO Method and the Electronic Structure of Extended Systems. Series: Research Reports in Physics, ISBN: 978-3-662-02564-2. Springer Berlin Heidelberg (Berlin, Heidelberg), Edited by Helmut Eschrig*, 1989.

[18] H Eschrig and I Bergert. An optimized lcao version for band structure calculations application to copper. *physica status solidi (b)*, 90(2):621–628, 1978.

[19] G Seifert, H Eschrig, and W Bieger. An approximation variant of lcao-x-alpha methods. *Zeitschrift Fur Physikalische Chemie-Leipzig*, 267(3):529–539, 1986.

[20] John C Slater and George F Koster. Simplified lcao method for the periodic potential problem. *Physical Review*, 94(6):1498, 1954.

[21] Dirk Porezag, Th Frauenheim, Th Köhler, Gotthard Seifert, and R Kaschner. Construction of tight-binding-like potentials on the basis of density-functional theory: Application to carbon. *Physical Review B*, 51(19):12947, 1995.

[22] Balint Aradi, Ben Hourahine, and Th Frauenheim. Dftb+, a sparse matrix-based implementation of the dftb method. *The Journal of Physical Chemistry A*, 111(26):5678–5684, 2007.

[23] Arnaud Fihey, Christian Hettich, Jérémy Touzeau, François Maurel, Aurélie Perrier, Christof Köhler, Bálint Aradi, and Thomas Frauenheim. Scc-dftb parameters for simulating hybrid gold-thiolates compounds. *Journal of computational chemistry*, 36(27):2075–2087, 2015.

[24] Xiaohang Lin and Axel Groß. First-principles study of the water structure on flat and stepped gold surfaces. *Surface Science*, 606(11-12):886–891, 2012.

[25] Ask Hjorth Larsen, Jens Jørgen Mortensen, Jakob Blomqvist, Ivano E Castelli, Rune Christensen, Marcin Dułak, Jesper Friis, Michael N Groves, Bjørk Hammer, Cory Hargus, et al. The atomic simulation environment: a python library for working with atoms. *Journal of Physics: Condensed Matter*, 29(27):273002, 2017.

[26] Berni J Alder and T E Wainwright. Studies in molecular dynamics. i. general method. *The Journal of Chemical Physics*, 31(2):459–466, 1959.

[27] W Matthew C Foulkes and Roger Haydock. Tight-binding models and density-functional theory. *Physical review B*, 39(17):12520, 1989.

[28] Nicholas Metropolis and Stanislaw Ulam. The monte carlo method. *Journal of the American statistical association*, 44(247):335–341, 1949.

[29] Bruce J Palmer. Direct application of shake to the velocity verlet algorithm. *Journal of Computational Physics*, 104(2):470–472, 1993.

[30] Dudley E Littlewood. Invariant theory, tensors and group characters. *Phil. Trans. R. Soc. Lond. A*, 239(807):305–365, 1944.

[31] Haruo Yoshida. Construction of higher order symplectic integrators. *Physics letters A*, 150(5-7):262–268, 1990.

[32] John Charles Butcher. The numerical analysis of ordinary differential equations: Runge-kutta and general linear methods. 1987.

[33] Karl E Petersen. *Ergodic theory*, volume 2. Cambridge university press, 1989.

[34] Gianluca Fazio, Gotthard Seifert, Mathias Rapacioli, Nathalie Tarrat, and Jan-Ole Joswig. Surface-charge dependent orientation of water at the interface of a gold electrode: A cluster study. *Zeitschrift für Physikalische Chemie*, pages 3–8, 2018.

[35] Martin Hangaard Hansen, Chengjun Jin, Kristian Sommer Thygesen, and Jan Rossmeisl. Finite bias calculations to model interface dipoles in electrochemical cells at the atomic scale. *The Journal of Physical Chemistry C*, 120(25):13485–13491, 2016.

[36] Yujin Tong, François Lapointe, Martin Thämer, Martin Wolf, and R Kramer Campen. Hydrophobic water probed experimentally at the gold electrode/aqueous interface. *Angewandte Chemie International Edition*, 56(15):4211–4214, 2017.

[37] David Leonard Chapman. Li. a contribution to the theory of electrocapillarity. *The London, Edinburgh, and Dublin philosophical magazine and journal of science*, 25(148):475–481, 1913.

[38] Guillermo L Beltramo, Tatyana E Shubina, and Marc TM Koper. Oxidation of formic acid and carbon monoxide on gold electrodes studied by surface-enhanced raman spectroscopy and dft. *ChemPhysChem*, 6(12):2597–2606, 2005.

[39] John C Slater and George F Koster. Simplified lcao method for the periodic potential problem. *Physical Review*, 94(6):1498, 1954.

[40] DA Papaconstantopoulos and MJ Mehl. The slater–koster tight-binding method: a computationally efficient and accurate approach. *Journal of Physics: Condensed Matter*, 15(10):R413, 2003.

[41] Erich Runge and Eberhard KU Gross. Density-functional theory for time-dependent systems. *Physical Review Letters*, 52(12):997, 1984.

[42] Robert Warmbier and Ralf Schneider. Ab initio potential energy surface of ch+ 2 and reaction dynamics of h+ ch+. *Physical Chemistry Chemical Physics*, 13(21):10285–10294, 2011.

[43] Robert Warmbier, Nkosinathi Malaza, and Alexander Quandt. Double-layer capacitance for a charged surface. *Ionics*, 23(2):331–335, 2017.

[44] Johannes Hachmann, Roberto Olivares-Amaya, Adrian Jinich, Anthony L Appleton, Martin A Blood-Forsythe, Laszlo R Seress, Carolina Roman-Salgado, Kai Trepte, Sule Atahan-Evrenk, Süleyman Er, et al. Lead candidates for high-performance organic photovoltaics from high-throughput quantum chemistry–the harvard clean energy project. *Energy & Environmental Science*, 7(2):698–704, 2014.

[45] ME Glavin, Paul KW Chan, S Armstrong, and WG Hurley. A stand-alone photovoltaic supercapacitor battery hybrid energy storage system. In *Power Electronics and Motion Control Conference, 2008. EPE-PEMC 2008. 13th*, pages 1688–1695. IEEE, 2008.

[46] Otto Stern. The theory of the electrolytic double-layer. *Z. Elektrochem*, 30(508):1014–1020, 1924.

[47] Alfred Rufer and Philippe Barrade. A supercapacitor-based energy-storage system for elevators with soft commutated interface. *IEEE Transactions on industry applications*, 38(5):1151–1159, 2002.

[48] Mark J Eddowes, H Allen O Hill, and K Uosaki. Electrochemistry of cytochrome c. comparison of the electron transfer at a surface-modified gold electrode with that to cytochrome oxidase. *Journal of the American Chemical Society*, 101(23):7113–7114, 1979.

[49] Muhammad Tanzirul Alam, Md Mominul Islam, Takeyoshi Okajima, and Takeo Ohsaka. Measurements of differential capacitance in room temperature ionic liquid at mercury, glassy carbon and gold electrode interfaces. *Electrochemistry Communications*, 9(9):2370–2374, 2007.

[50] Aldo Di Carlo, Alessandro Pecchia, Luca Latessa, Th Frauenheim, and Gotthard Seifert. Tight-binding dft for molecular electronics (gdftb). In *Introducing Molecular Electronics*, pages 153–184. Springer, 2006.

[51] Li Li Zhang and XS Zhao. Carbon-based materials as supercapacitor electrodes. *Chemical Society Reviews*, 38(9):2520–2531, 2009.

[52] Robert D Skeel, Guihua Zhang, and Tamar Schlick. A family of symplectic integrators: stability, accuracy, and molecular dynamics applications. *SIAM Journal on Scientific Computing*, 18(1):203–222, 1997.

[53] N Metropolis. Monte carlo method. *From Cardinals to Chaos: Reflection on the Life and Legacy of Stanislaw Ulam*, page 125, 1989.

[54] M Germana Paterlini and David M Ferguson. Constant temperature simulations using the langevin equation with velocity verlet integration. *Chemical Physics*, 236(1-3):243–252, 1998.

[55] Lianrui Zhang, H Ted Davis, DM Kroll, and Henry S White. Molecular dynamics simulations of water in a spherical cavity. *The Journal of Physical Chemistry*, 99(9):2878–2884, 1995.

[56] Richard Car and Mark Parrinello. Unified approach for molecular dynamics and density-functional theory. *Physical review letters*, 55(22):2471, 1985.

[57] Enrico Fermi, John R Pasta, and Stanislaw M Ulam. Studies of nonlinear problems. 1955.

[58] Emily A Carter. 2005 american conference on theoretical chemistry. Technical report, Regents of the University of California, 2006.

[59] Josue A Lopez-Berganza, Yijue Diao, Sudhakar Pamidighantam, and Rosa M Espinosa-Marzal. Ab initio studies of calcium carbonate hydration. *The Journal of Physical Chemistry A*, 119(47):11591–11600, 2015.

[60] Jean-Sébastien Filhol and Matthew Neurock. Elucidation of the electrochemical activation of water over pd by first principles. *Angewandte Chemie International Edition*, 45(3):402–406, 2006.

[61] Deivasigamani Umadevi, Swati Panigrahi, and Garikapati Narahari Sastry. Noncovalent interaction of carbon nanostructures. *Accounts of chemical research*, 47(8):2574–2581, 2014.

[62] Muhammad Faheem and Andreas Heyden. Hybrid quantum mechanics/molecular mechanics solvation scheme for computing free energies of reactions at metal–water interfaces. *Journal of chemical theory and computation*, 10(8):3354–3368, 2014.

[63] Juan-Jesus Velasco-Velez, Cheng Hao Wu, Tod A Pascal, Liwen F Wan, Jinghua Guo, David Prendergast, and Miquel Salmeron. The structure of interfacial water on gold electrodes studied by x-ray absorption spectroscopy. *Science*, page 1259437, 2014.

[64] Ch Köhler, G Seifert, U Gerstmann, M Elstner, H Overhof, and Th Frauenheim. Approximate density-functional calculations of spin densities in large molecular systems and complex solids. *Physical Chemistry Chemical Physics*, 3(23):5109–5114, 2001.

[65] M Gouy. Sur la constitution de la charge électrique à la surface d'un électrolyte. *J. Phys. Theor. Appl.*, 9(1):457–468, 1910.

[66] ND Lang and W Kohn. Theory of metal surfaces: charge density and surface energy. *Physical Review B*, 1(12):4555, 1970.

[67] Christopher D Taylor, Sally A Wasileski, Jean-Sebastien Filhol, and Matthew Neurock. First principles reaction modeling of the electrochemical interface: Consideration and calculation of a tunable surface potential from atomic and electronic structure. *Physical Review B*, 73(16):165402, 2006.

[68] George D Birkhoff. Proof of the ergodic theorem. *Proceedings of the National Academy of Sciences*, 17(12):656–660, 1931.

[69] Ludwig Boltzmann. *Vorlesungen über gastheorie*, volume 1. JA Barth, 1896.

[70] H By Helmholtz. Studies on electrical boundary layers. *Annalen der Physik*, 243(7):337–382, 1879.

[71] Adam P Willard, Stewart K Reed, Paul A Madden, and David Chandler. Water at an electrochemical interface?a simulation study. *Faraday discussions*, 141:423–441, 2009.

[72] Ken-ichi Ataka, Takao Yotsuyanagi, and Masatoshi Osawa. Potential-dependent reorientation of water molecules at an electrode/electrolyte interface studied by surface-enhanced infrared absorption spectroscopy. *The Journal of Physical Chemistry*, 100(25):10664–10672, 1996.

[73] Pavel Jungwirth. Spiers memorial lecture ions at aqueous interfaces. *Faraday discussions*, 141:9–30, 2009.

[74] Roger Parsons. The electrical double layer: recent experimental and theoretical developments. *Chemical Reviews*, 90(5):813–826, 1990.

[75] Wolfgang Schmickler and Douglas Henderson. New models for the structure of the electrochemical interface. *Progress in Surface Science*, 22(4):323–419, 1986.

[76] Th Frauenheim, G Seifert, M Elsterner, Z Hajnal, G Jungnickel, D Porezag, S Suhai, and R Scholz. A self-consistent charge density-functional based tight-binding method for predictive materials simulations in physics, chemistry and biology. *physica status solidi(b)*, 217(1):41–62, 2000.

[77] Walter Kohn and Lu Jeu Sham. Self-consistent equations including exchange and correlation effects. *Physical review*, 140(4A):A1133, 1965.

[78] Weitao Yang and Paul W Ayers. Density-functional theory. In *Computational Medicinal Chemistry for Drug Discovery*, pages 103–132. CRC Press, 2003.

[79] Marcus Elstner, Dirk Porezag, G Jungnickel, J Elsner, M Haugk, Th Frauenheim, Sandor Suhai, and Gotthard Seifert. Self-consistent-charge density-functional tight-binding method for simulations of complex materials properties. *Physical Review B*, 58(11):7260, 1998.

[80] Marcus Elstner and Gotthard Seifert. Density functional tight binding. *Philosophical Transactions of the Royal Society A: Mathematical, Physical and Engineering Sciences*, 372(2011):20120483, 2014.

[81] Pekka Koskinen and Ville Mäkinen. Density-functional tight-binding for beginners. *Computational Materials Science*, pages 237–253, 2009.

Appendix A

Ergodic Hypothesis

A.1 Ergodic Hypothesis and Theorem

One of the most powerful principles in physics is the principle of the equipartition of energy in a system. Which states that, over long periods of time, the energy of a system would equally distribute itself over all the degrees of freedom of the system, i.e., all accessible microstates of the system are equiprobable, given a sufficiently long period of time. And thus, roughly, the time average and the space average are equivalent. As powerful as the principle of the equipartition of energy is, it can only hold true for certain conditions, one of which it hinges upon greatly is the Ergodic Hypothesis, Initially proposed by Ludwig Boltzmann [69]. What the Ergodic Hypothesis states is that over long periods of time, the time that is spent in an arbitary region of the phase space of microstates, with the same energy, is proportional to the volume of this arbitary region. Using insights from this hypothesis and combining that with measure theory, George Birkhoff, in principle, solved this fundamental problem of statistical mechanics and came up with the *Ergodic Theorem* [68]. The proof is as follows:

The collection of all states of a system forms a phase space X. The evolution of a system takes the form $T : X \to X$, which is a measure-preserving transformation on a measure space (X, Γ, μ), the trajectory $T^n x : n \in \mathbb{Z}$ of a point $x \in X$ represents a single complete history of a system and, lastly, let us suppose that $f : X \to \mathbb{R}$, represents a measurement made on the system, is a $\mu-$integrable. Now we can define the following averages:

Time Average:

$$\hat{f}(x) = \lim_{n\to\infty} \frac{1}{n} \sum_{k=0}^{n-1} f\left(T^k x\right) \tag{A.1}$$

Space Average:

$$\bar{f} = \frac{1}{X} \int f d\mu \tag{A.2}$$

Assuming that X is finite and non-zero, for a probability space, $X = 1$. The *Pointwise theorem* [33] states that the limit in our definition of the time average exists for almost every x and that the "just about everywhere defined" limit $\hat{f}$ is integrable and T-invariant:

$$\hat{f} \in L^1(\mu) \qquad \hat{f} \circ T = \hat{f} \tag{A.3}$$

And thus holds almost everywhere:

$$\int \hat{f} d\mu = \int f d\mu \tag{A.4}$$

If T is ergodic, then $\hat{f}$ must be constant just about everywhere and so we have that $\bar{f} = \hat{f}$ just about everywhere. If we consolidate all our claims we arrive to:

$$\lim_{n\to\infty} \frac{1}{n} \sum_{k=0}^{n-1} f\left(T^k x\right) = \frac{1}{X} \int f d\mu \tag{A.5}$$

for almost all x, except for a negligible amount.